https://doi.org/10.1093/plcell/koad089 THE PLANT CELL 2023: 35: 2208–2231

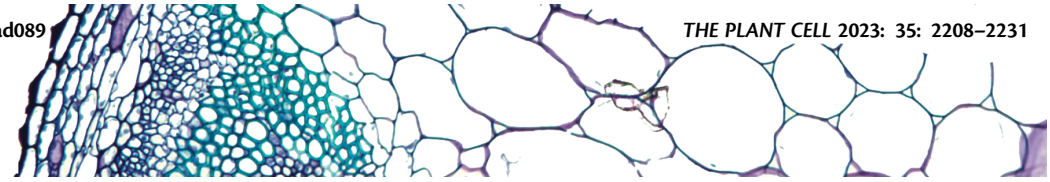

Research Article

INDETERMINATE1 autonomously regulates phosphate homeostasis upstream of the miR399-*ZmPHO2* signaling module in maize

Xufeng Wang [1,2,3,†] **Dan Yuan** [1,2,†] **Yanchun Liu** [1,2] **Yameng Liang** [4] **Juan He** [1,2] **Xiaoyu Yang** [1,2,5] **Runlai Hang** [3] **Hong Jia** [4] **Beixin Mo** [1] **Feng Tian** [4] **Xuemei Chen** [3,*] **and Lin Liu** [1,*]

1 Guangdong Provincial Key Laboratory for Plant Epigenetics, Longhua Bioindustry and Innovation Research Institute, College of Life Sciences and Oceanography, Shenzhen University, Shenzhen, Guangdong 518060, China
2 Key Laboratory of Optoelectronic Devices and Systems of Ministry of Education and Guangdong Province, College of Optoelectronic Engineering, Shenzhen University, Shenzhen, Guangdong 518060, China
3 Department of Botany and Plant Sciences, Institute of Integrative Genome Biology, University of California, Riverside, CA 92521, USA
4 State Key Laboratory of Plant Physiology and Biochemistry, National Maize Improvement Center, Key Laboratory of Biology and Genetic Improvement of Maize (MOA), Beijing Key Laboratory of Crop Genetic Improvement, China Agricultural University, Beijing 100193, China
5 College of Horticulture Science and Engineering, Shandong Agricultural University, Taian 271018, China

*Author for correspondence: linliu@szu.edu.cn (L.L.), xuemei.chen@ucr.edu (X.C.)
†These authors contributed equally.
The author responsible for distribution of materials integral to the findings presented in this article in accordance with the policy described in the Instructions for Authors (https://academic.oup.com/plcell/pages/General-Instructions) is: Lin Liu (linliu@szu.edu.cn).

Abstract

The macronutrient phosphorus is essential for plant growth and development. Plants have evolved multiple strategies to increase the efficiency of phosphate (Pi) acquisition to protect themselves from Pi starvation. However, the crosstalk between Pi homeostasis and plant development remains to be explored. Here, we report that overexpressing microRNA399 (miR399) in maize (*Zea mays*) is associated with premature senescence after pollination. Knockout of *ZmPHO2* (*Phosphate 2*), a miR399 target, resulted in a similar premature senescence phenotype. Strikingly, we discovered that INDETERMINATE1 (ID1), a floral transition regulator, inhibits the transcription of *ZmMIR399* genes by directly binding to their promoters, alleviating the repression of *ZmPHO2* by miR399 and ultimately contributing to the maintenance of Pi homeostasis in maize. Unlike *ZmMIR399* genes, whose expression is induced by Pi deficiency, *ID1* expression was independent of the external inorganic orthophosphate status, indicating that ID1 is an autonomous regulator of Pi homeostasis. Furthermore, we show that *ZmPHO2* was under selection during maize domestication and cultivation, resulting in a more sensitive response to Pi starvation in temperate maize than in tropical maize. Our study reveals a direct functional link between Pi-deprivation sensing by the miR399-*ZmPHO2* regulatory module and plant developmental regulation by ID1.

Introduction

Phosphorus is present in every living cell and its functions cannot be substituted by other nutrients (Marschner 1995). As 1 of 17 essential nutrients, phosphorus is required for almost all developmental processes of plants and is considered to be 1 of 3 primary macronutrients, along with nitrogen and potassium (Bindraban et al. 2020). Nevertheless, most cultivated land worldwide has poor phosphorus availability, and levels of inorganic orthophosphate (Pi), which plants take up through their roots, are suboptimal

Received January 20, 2023. Accepted February 25, 2023. Advance access publication March 21, 2023

IN A NUTSHELL

Background: Phosphorus is an essential macronutrient for plant growth and development. To cope with phosphorus limitation, plants have evolved sophisticated strategies to coordinate phosphorus acquisition, scavenging, and recycling. Maize is an important crop and cultivated widely for both staple food and industrial usage. Although phosphorus is a major constituent of the fertilizers required to sustain high yields in maize, global phosphorus resources are quickly diminishing and may be exhausted in the near future.

Question: We sought to understand the underlying molecular mechanisms behind phosphate acquisition and utilization in maize to develop varieties with high-phosphorus use efficiency.

Findings: We observed that overexpressing microRNA399 (miR399) or knocking out of its target gene *ZmPHO2* results in an apparent leaf senescence phenotype after pollination. We further discovered that the transcription factor INDETERMINATE1 (ID1) functions as an autonomous upstream regulator of phosphorus homeostasis by suppressing the transcription of *ZmMIR399* genes, thus decreasing the accumulation of mature miR399 and alleviating the cleavage of *ZmPHO2* transcripts, ultimately contributing to the maintenance of phosphorus homeostasis in maize. Our work establishes a regulatory connection between phosphorus nutrient homeostasis and vegetative–reproductive development in maize. More importantly, we show that *ZmPHO2* underwent strong selection during maize domestication and cultivation. This study provides genetic resources for improving maize phosphorus use efficiency and breeding low phosphorus-tolerant maize varieties by editing the *ID1*-miR399-*ZmPHO2* module.

Next steps: We will attempt to generate *ID1*-modified plants to fine-tune flowering time and phosphorus uptake in maize. The specific functions of each *MIR399* family member may also be interrogated by generating genome-edited mutants. As we discovered that *Bx* genes involved in benzoxazinoid biosynthesis are also affected by miR399, we hope to further explore the mechanism of miR399 functioning as a negative regulator of plant immunity.

in soils for vegetative growth and crop productivity (Raghothama 1999; López-Arredondo et al. 2014). Along with other fertilizers, Pi must be routinely applied to farmland to support healthy crop growth. However, Pi fertilizers used for agriculture are mostly produced from mined rock Pi, which is nonrenewable and predicted to decline in availability before the end of this century (Vance et al. 2003; Baker et al. 2015). Thus, modifying crop plants to make them amenable to soils with a restricted supply of Pi is vital if high crop yields, which are necessary to support the food demands of a continuously increasing world population, are to be maintained.

Pi-efficient plants would reduce the requirement for Pi fertilizers, thereby ameliorating their overuse while concurrently enhancing yield. The investigation and manipulation of genes involved in Pi acquisition, remobilization, and metabolism are potential strategies for the development of Pi-efficient crops, which might facilitate agricultural sustainability. To date, a series of Pi starvation-related genes and regulators have been characterized in the model plant Arabidopsis (*Arabidopsis thaliana*), including genes encoding transcription factors such as PHOSPHATE STARVATION RESPONSE1 (PHR1) (Rubio et al. 2001; Maeda et al. 2018), PHR1-LIKE1 (Bustos et al. 2010), WRKY75 and ZAT6 (Devaiah and Raghothama 2007; Devaiah et al. 2007a; Devaiah et al. 2007b), the long noncoding RNA *INDUCED BY PHOSPHATE STARVATION1* (*IPS1*) (Franco-Zorrilla et al. 2007), microRNA399 (miR399) (Bari et al. 2006; Chiou et al. 2006; Pant et al. 2008), and members of the *PHOSPHATE* (*PHO*) gene family (Aung et al. 2006; Stefanovic et al. 2007). In particular, *PHO2* (*Phosphate 2*), which encodes a ubiquitin-conjugating E2 enzyme (UBC), is known to be a miR399 target and is involved in Pi homeostasis (Bari et al. 2006). Under Pi-sufficient conditions, PHO2 targets Pi transporters for poly-ubiquitination and degradation, thereby maintaining optimal Pi uptake (Liu et al. 2012; Li et al. 2017; Sega et al. 2020). By contrast, Pi deficiency stress induces miR399 accumulation, which downregulates the abundance of *PHO2* transcripts via cleavage (Bari et al. 2006), in turn allowing the accumulation of Pi transporters to enhance Pi acquisition and translocation (Aung et al. 2006). The miR399-*PHO2* module also regulates Pi homeostasis in rice (*Oryza sativa*), maize (*Zea mays*), wheat (*Triticum aestivum*), and other species (Chiou et al. 2006; Hu et al. 2011; Xu et al. 2013; Du et al. 2018). Long noncoding RNAs *PILNCR1* (*Pi-deficiency-induced long noncoding RNA1*) in maize, or *IPS1* in Arabidopsis, serve as miR399 sponges to reduce miR399-guided cleavage of *PHO2* RNA and help plants adapt to Pi deficiency (Franco-Zorrilla et al. 2007; Du et al. 2018). Previous studies have demonstrated that the induction of *MIR399* under Pi-limited conditions is repressed in an Arabidopsis mutant, *phr1* (Bari et al. 2006), showing that PHR1 functions as an upstream regulator of miR399 in the Pi-deprivation response. Similarly, overexpression of *ZmPHR1* in maize or *OsPHR1* and *OsPHR2* in rice resulted in increased Pi uptake ability and elevated Pi content under Pi-limited conditions (Zhou et al. 2008; Wang et al. 2013b). Although PHR1, miR399, and PHO2 define a conserved regulatory module that

maintains Pi homeostasis in various plant species (Bari et al. 2006), other transcription factors, such as OsPTF1 (Pi starvation-induced transcription factor 1) in rice and ZmPTF1 in maize, have also been functionally characterized with respect to low-Pi stress responses (Yi et al. 2005; Li et al. 2011). Even so, characterizing more genes involved in Pi homeostasis and elucidating their regulatory networks could help improve phosphorus use efficiency to facilitate plant acclimation to changing Pi environments.

Maize is not only an important crop for food and feed but also a source of primary compounds for industrial innovation (Andorf et al. 2019). It has been widely cultivated in tropical and temperate soils worldwide, following domestication from its wild progenitor, teosinte *parviglumis* (*Z. mays* ssp. *parviglumis*), which was originally grown in the lowland, subtropical environment of the Balsas River basin (Guerrero, México) (Matsuoka et al. 2002). In the early stage of domestication, adaptation of *parviglumis* from the lowland environments to low temperature and soils with low phosphorus content in highland environments drove the genetic divergence between *parviglumis* and *mexicana* (*Z. mays* ssp. *Mexicana*, another teosinte subspecies) (Aguirre-Liguori et al. 2019; Barnes et al. 2022), suggesting that the soil phosphorus status is a key driver of local adaptation in maize. Under current cultivation conditions, especially in acidic and alkaline soils, large amounts of Pi fertilizers are applied to maize fields, allowing maize plants to become well-established and mature in a suitable timeframe, thus improving overall yield (Khan et al. 2020; Qaswar et al. 2020). However, despite these advantages, the long-term use of large amounts of fertilizers might weaken the nutrient (such as Pi) uptake systems of plants during cultivation (Liu et al. 2021). Thus, research on Pi regulators is needed, with the ultimate aim of optimizing the acquisition and use of Pi by plants.

Here, we report that overexpressing miR399 in maize resulted in typical Pi toxicity phenotypes, as manifested by premature senescence in mature leaves after pollination. We also generated *Zmpho2* mutants by clustered regularly interspaced short palindromic repeat (CRISPR)/CRISPR-associated nuclease 9 (Cas9)-mediated editing and determined that knocking out the *ZmPHO2* gene, a miR399 target, consistently produced a premature leaf senescence phenotype similar to that of the transgenic miR399-overexpression lines. Transcriptome profiling and targeted metabolite measurements in miR399-overexpression and miR399-knockdown transgenic lines revealed that, in addition to affecting the Pi response and leaf senescence, miR399 might mediate pathogen and insect defense in maize by regulating the expression of *Bx* genes in the benzoxazinoid biosynthesis pathway. We further demonstrated that an upstream regulator of the miR399-*ZmPHO2* module, INDETERMINATE1 (ID1), can inhibit the transcription of *ZmMIR399* genes and hence the accumulation of mature miR399, to alleviate the repression of *ZmPHO2* by miR399, and ultimately maintain Pi homeostasis in maize. *ID1* expression was unperturbed by low-Pi stress, suggesting that ID1 acts as an autonomous Pi regulator in maize. We conclude that mutation of *ID1* triggers the miR399-*ZmPHO2* pathway, a conserved Pi response module in plants, to promote Pi acquisition, providing the necessary Pi supply to support the vegetative gigantism of the *id1* mutant. We also showed that *ZmPHO2* was under selection during maize domestication and cultivation, resulting in a more sensitive response to Pi starvation in temperate maize than tropical maize. We speculate that, during maize domestication or subsequent cultivation, Pi uptake ability might have degenerated as maize spread into high-Pi environments, resulting from prolonged and excessive Pi application in pursuit of improvements in yield. Our study establishes a regulatory connection between nutrient homeostasis and vegetative development in maize.

Results

Transgenic maize plants overexpressing miR399 display an apparent leaf senescence phenotype after pollination

The miR399 family in maize contains a total of 10 members (i.e. miR399a-j) generated by ten *ZmMIR399* genes and can be divided into 6 subgroups based on their respective mature miRNA sequences (Zhang et al. 2009) (Supplemental Fig. S1). To investigate the biological roles of the miR399 family in maize, we subcloned 2 types of mature 21-nt miR399 sequences (miR399a/c/h and miR399e/i/j) in the same vector using a 2-hit artificial miRNA design (Supplemental Fig. S2A). Because the mature miR399 species have very similar sequences (Supplemental Fig. S1A) and certain mismatches between a miRNA and its target sequence are allowed (Bologna and Voinnet 2014), this overexpression construct probably represents the overexpression of the entire miR399 family. We chose 3 independent transgenic lines (named miR399-OE#1, miR399-OE#2, and miR399-OE#3) for experiments after confirming the accumulation of mature miR399 by RNA gel blot analysis (Fig. 1A). The total phosphorus content was significantly higher in shoots of miR399-overexpressing transgene-positive plants (miR399-OEP#1-#3) compared with their isogenic siblings without the transgene, i.e. miR399 transgene-negative plants (miR399-OEN#1-#3) derived from the same transformation event (Fig. 1B; Supplemental Fig. S3, A and B), suggesting that accumulation of miR399 induces enhanced Pi acquisition. By contrast, we observed no significant difference for phosphorus content in roots of transgene-positive and transgene-negative plants, resulting in a higher shoot-to-root Pi content ratio in miR399-overexpressing transgene-positive plants (Fig. 1B; Supplemental Fig. S3, A and B). Consistent with a previous report (Du et al. 2018), leaf necrosis at the margins of old leaves appeared at the seedling stage of miR399-overexpressing transgene-positive plants grown in hydroponic solution with a sufficient Pi supply (Supplemental Fig. S4); this phenotype was previously

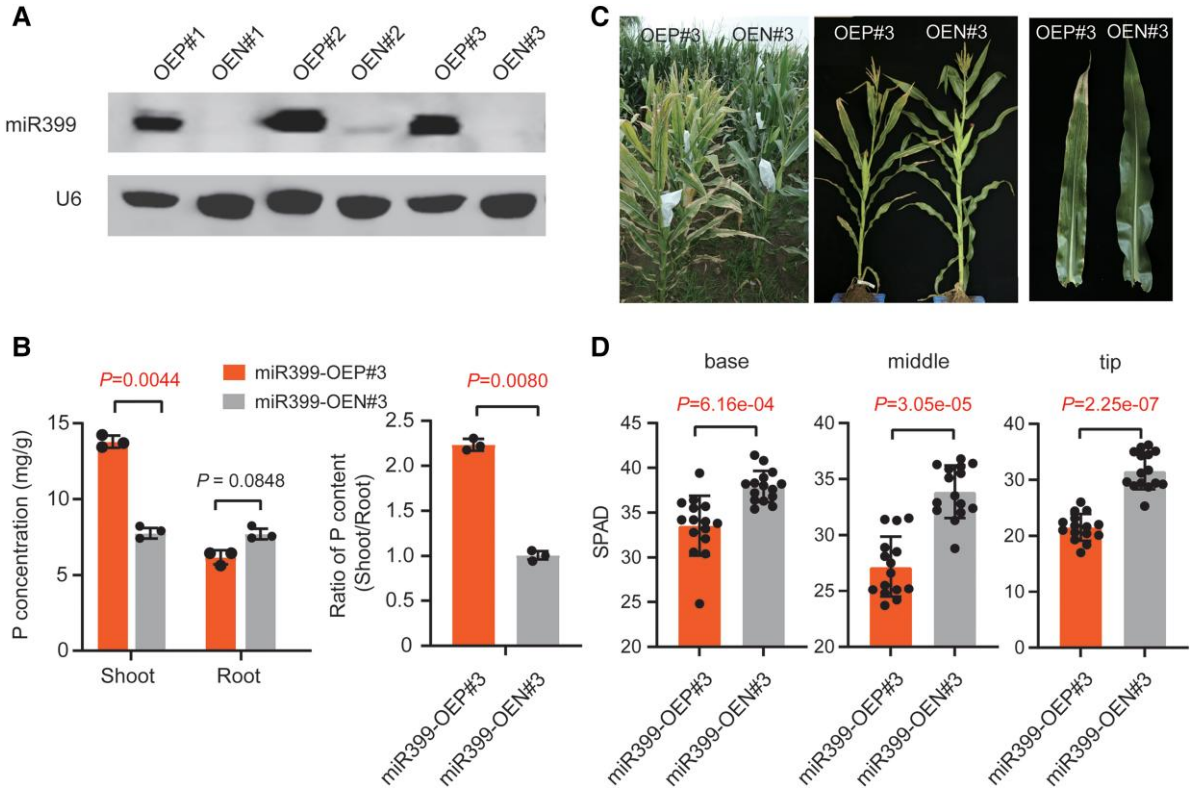

Figure 1. Phenotype of field-grown miR399-overexpressing transgenic plants. **A)** RNA gel blot showing that mature miR399 accumulates in 3 independent transgenic lines (named OEP#1–OEP#3). A total of 10 μg total RNA from seedlings of each line was loaded per lane, and the membrane was hybridized with a biotin-labeled miR399 probe. U6 served as a loading control. OEP and OEN represent transgene-positive and transgene-negative plants, respectively, derived from the same transformation event. **B)** Total phosphorus (P) contents in shoots and roots of miR399-OEP and miR399-OEN lines. A representative transgenic strain, miR399-OE#3, was chosen and 3 biological replicates for each genotype were prepared for total P concentration measurement. Values are means ± SD; the *P*-values were determined by Student's *t*-test (Supplemental Data Set S6). **C)** Premature senescence phenotypes of miR399-OEP#3 and miR399-OEN#3 plants grown in the field. A field scene and representative plants at 15 d after pollination are shown. **D)** Quantification of total chlorophyll content (shown as SPAD values) in different parts (base, middle, and tip) of mature ear leaves from miR399-OEP#3 and miR399-OEN#3 after pollination. A total of 15 plants were measured for chlorophyll content for each genotype. Values are means ± SD; the *P*-values were determined by Student's *t*-test (Supplemental Data Set S6). SPAD represents total chlorophyll content, which was measured with a Konica Minolta SPAD 502 Plus instrument.

reported to be a typical Pi-toxicity phenotype (Du et al. 2018). To investigate whether miR399 accumulation affects maize developmental and agronomic traits, we grew 3 independent miR399-overexpression lines in the field (Liaoning, 41.8° N, 123.4° E) along with their corresponding isogenic control siblings. All 3 miR399 overexpression transgene-positive lines showed markedly earlier leaf senescence than their corresponding transgene-negative siblings, especially after pollination (Fig. 1C; Supplemental Fig. S3, C and D), but did not exhibit any significant differences on agronomic traits (Supplemental Fig. S5). Concomitantly, the miR399-overexpression transgenic lines showed significantly lower chlorophyll content across the entire mature leaf, from base to tip (Fig. 1D; Supplemental Fig. S3, E and F). Collectively, these results indicate that miR399 functions as a positive regulator of phosphorus uptake and that overexpression of miR399 induces an apparent premature senescence syndrome after pollination in maize.

Short tandem target mimicry (STTM) technology (Tang et al. 2012; Tang and Tang 2013), which was developed as an improvement upon the original target mimicry approach, is an effective tool to block miRNA activity or cause miRNA degradation (Peng et al. 2018). The STTM construct usually contains 2 imperfect miRNA target sites with a CTA trinucleotide bulge in the center linked by a 31-nt to 96-nt short spacer (Yan et al. 2012). To generate miR399-knockdown transgenic plants (miR399-STTM), we designed a STTM construct containing 2 noncleavable miR399-binding sites targeting 2 different mature miR399 species corresponding to miR399a/c/h and miR399e/i/j (Supplemental Fig. S2B). The abundance of miR399 decreased in 2 independent miR399-STTM transgene-positive lines (miR399-STTMP#1 and miR399-STTMP#2) compared with their isogenic transgene-free siblings (miR399-STTMN#1 and miR399-STTMN#2), confirming the successful knockdown of endogenous miR399 (Supplemental Fig. S6A). However, phosphorus accumulation in shoots was

not significantly different between miR399-STTM transgene-positive and transgene-negative lines (Supplemental Fig. S6B). The lack of a change in phosphorus content might be due to the naturally low levels of miR399 at the seedling stage under normal growth conditions, which would minimize any differences in miR399 levels between miR399-STTMP and miR399-STTMN lines. We thus grew homozygous miR399-STTMP transgenic lines in the field (Liaoning, 41.8° N, 123.4° E) for phenotypic observation along with their corresponding isogenic control siblings. We observed no visible developmental or morphological differences between the transgene-positive and their corresponding transgene-negative lines (Supplemental Fig. S6C), suggesting that a minor reduction in miR399 levels does not affect maize development under normal conditions. Growing miR399-STTM plants under Pi-sufficiency/-deficiency soil regimes needs to be performed in the future for further phenotypic characterization.

Knocking out *ZmPHO2*, a miR399 target, results in premature senescence

PHO2, which encodes a UBC enzyme, has been experimentally confirmed to be a target of miR399 in various species, including Arabidopsis, rice, barley (*Hordeum vulgare*), soybean (*Glycine max*), and maize (Fujii et al. 2005; Bari et al. 2006; Chiou et al. 2006; Pant et al. 2008; Hu et al. 2011; Hackenberg et al. 2013; Xu et al. 2013; Du et al. 2018). In maize, miR399b directs the cleavage of *ZmPHO2* mRNA, which contains 6 tandem miR399-binding sites in its 5′ untranslated region (5′ UTR) (Fig. 2A), based on transient expression, and 5′ rapid amplification of cDNA ends (5′ RACE) assays (Du et al. 2018). To validate this relationship for other miR399s, we performed transient coexpression assays in maize protoplasts with different miR399 precursors as effectors, together with a firefly luciferase (LUC) reporter construct harboring the 5′ UTR of *ZmPHO2* upstream of *LUC* and downstream of a minimal cauliflower mosaic virus (CaMV) 35S promoter (Supplemental Fig. S7A). Besides the observation that miR399b significantly repressed the activity of LUC derived from the reporter construct, we confirmed that miR399a/c/h, miR399e/i/j, and miR399f significantly inhibit LUC activity (Supplemental Fig. S7B), suggesting that these miR399 species can act through the miR399-binding sites in the 5′ UTR of *ZmPHO2*. We examined *ZmPHO2* expression by RT-qPCR in miR399-OE and miR399-STTM transgenic lines and observed the expected expression changes, with significant downregulation and upregulation in miR399-OE and miR399-STTM transgenic lines, respectively (Fig. 2B), demonstrating that *ZmPHO2* is an authentic target of miR399. However, so far, we lack genetic evidence for the function of *ZmPHO2* in the regulation of Pi homeostasis and plant development in maize. To examine the function of *ZmPHO2*, we knocked out *ZmPHO2* in the maize inbred line ZZC01 using CRISPR/Cas9-mediated mutagenesis (Doudna and Charpentier 2014; Belhaj et al. 2015; Ma et al. 2015). We noticed that the annotations of *ZmPHO2* show different gene structures among different versions of the maize genome (GRMZM2G381709 in AGPv3, Zm00001d038972 in AGPv4, and Zm0001eb295490 in AGPv5; Supplemental Fig. S8). We thus used public RNA-seq data and transcription start site data to reevaluate the gene structure of *ZmPHO2* (Supplemental Fig. S8). We determined that the gene structures annotated by Du et al. (2018) and AGPv5 highly agree, with the same translation start site and similar exon–intron junctions, and thus adopted this annotation for generating knockout mutants (Supplemental Fig. S8). We designed 2 single-guide RNAs (sgRNAs) to target the coding region immediately after the translation start site within the first exon of *ZmPHO2* (Fig. 2A). Genotyping and sequence analyses identified 3 homozygous mutants harboring fragment insertions and/or deletions around the sgRNA target sites (Fig. 2C). The 3 homozygous, potentially null mutants consistently showed a typical Pi toxicity phenotype and exhibited premature senescence (Fig. 2D). The leaf senescence phenotypes were more severe than those of the miR399-OE transgenic lines such that very few seeds could be harvested.

miR399 might mediate pathogen and insect defense in maize, in addition to affecting Pi response and leaf senescence

To characterize the gene network(s) through which miR399 might influence maize development and physiology, we carried out a comparative transcriptome analysis of mature leaves (V5 stage) between homozygous miR399-OEP#3 and miR399-STTMP#2 and their corresponding transgene-negative siblings (miR399-OEN#3 and miR399-STTMN#2) with 3 replicates, which showed high reproducibility (Supplemental Fig. S9). By comparison to their corresponding transgene-negative siblings, we identified 2,559 and 1,480 differentially expressed genes (DEGs) in miR399-OE#3 and miR399-STTM#2, respectively (fold change ≥ 1.5 & FDR ≤ 0.05; Fig. 3A; Supplemental Data Sets S1 and S2). Annotating these DEGs highlighted some genes involved in Pi homeostasis, such as the Pi transporters *ZmPT2* (*Phosphate transporter 2*) (Vasconcelos et al. 2022) and *ZmPHO1;2b* (*Phosphate transporter PHO1-2-like*) (Ma et al. 2021), as well as the Pi-salvaging/recycling genes *ZmPAP21* (*Purple acid phosphatase 21*) (González-Muñoz et al. 2015) and *ZmGPX-PDE9/11/14* (*Glycerophosphodiester phosphodiesterase 9/11/14*) (Wang et al. 2021) (Supplemental Data Sets S1 and S2), and some leaf senescence-associated genes, including *SAG12* (*Senescence-associated gene 12*) and transcription factor genes belonging to the NAC and WRKY families (Breeze et al. 2011; Stigter and Plaxton 2015) (Supplemental Data Sets S1 and S2). In addition, Gene Ontology (GO) and Kyoto Encyclopedia of Genes and Genomes (KEGG) enrichment analyses showed that these DEGs are significantly enriched in GO terms or pathways associated with secondary metabolism, including oxylipin metabolism, lignin biosynthesis, and linoleic acid metabolism, to name a few (Supplemental Fig.

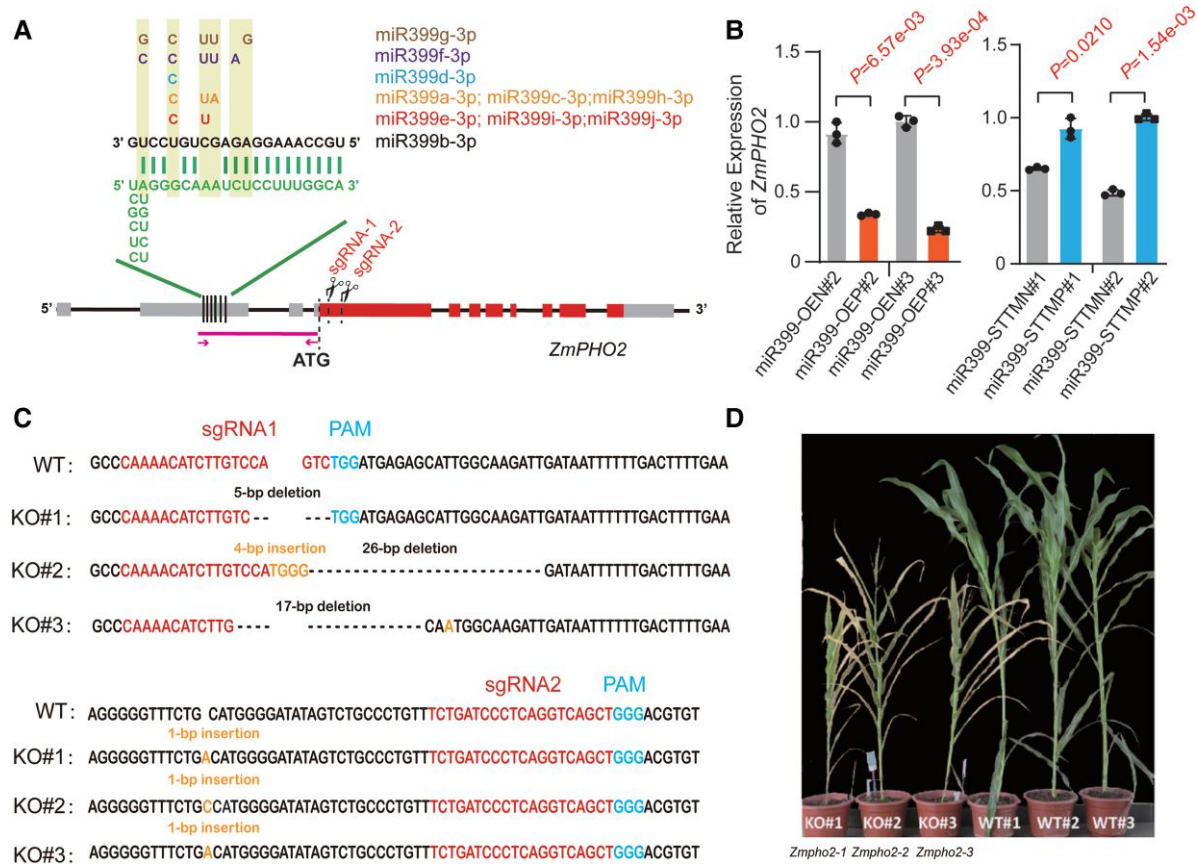

Figure 2. CRISPR/Cas9-mediated mutagenesis of *ZmPHO2* causes premature senescence in maize. **A)** Diagram of the *ZmPHO2* locus. Gray box, untranslated regions; red box, coding regions. Six predicted miR399 target sites (4 of them were experimentally validated by Du et al. (2018)) are located in the 5′ UTR. The sequences of the 6 sites are shown in green and those of the various miR399 members are shown in multiple colors. sgRNA-1 and sgRNA-2 represent 2 single-guide RNAs for CRISPR/Cas9-mediated editing. The magenta line segment with arrows indicates the 5′ UTR fragment used in dual-luciferase assays in Supplemental Fig. S7 and Fig. 7D. **B)** Relative *ZmPHO2* expression as determined by RT-qPCR in miR399-OE and miR399-STTM transgene-positive lines and the corresponding negative controls. The *P*-values were calculated by Student's *t*-test (Supplemental Data Set S6). *ZmPHO2* expression was normalized to that of *ZmUBI*. **C)** Sequences of 3 homozygous knockout lines with insertions/deletions that truncate the *ZmPHO2* open reading frame (named KO#1, KO#2, and KO#3). The wild-type (WT) sequence is shown at the top. sgRNA and protospacer-adjacent motif (PAM) sequences are in red and blue, respectively. The deletions are indicated by dashes, while the inserted nucleotides are shown in orange. **D)** Gross morphology of 3 *Zmpho2* knockout lines and 3 wild-type lines.

S10; Supplemental Data Sets S3 and S4). Of these DEGs, we defined 971 genes as downregulated DEGs (down-DEGs) in miR399-OE plants, with significantly lower expression levels in miR399-OEP#3 compared with miR399-OEN#3 (Fig. 3A). Similarly, we identified 729 upregulated DEGs (up-DEGs) in miR399-STTM plants, with significantly higher expression levels in miR399-STTMP#2 than in miR399-STTMN#2 (Fig. 3B). Overlap analysis between the down-DEGs in miR399-OE and up-DEGs in miR399-STTM identified a small subset of high-confidence genes (102 genes; Fig. 3C), whose expression was negatively correlated with miR399 levels. Detailed annotation of this small subset of genes revealed a number of Pi-related genes, including *ZmPHO2* (Fig. 3D; Supplemental Data Set S2). Pathway enrichment analysis of these miR399-associated genes in reference to the GO and KEGG databases showed that the term "benzoxazinoid biosynthesis" is the most strongly enriched (Fig. 3E).

Benzoxazinoids are a class of indole-derived protective and allelopathic secondary metabolites that are involved in antifungal and insect defense responses in plants (Frey et al. 2009). 2,4-Dihydroxy-1,4-benzoxazin-3-one (DIBOA) and its 7-methoxy analog 2,4-dihydroxy-7-methoxy-1,4-benzoxazin-3-one (DIMBOA) are the predominant benzoxazinoids in plants (Frey et al. 1997; Frey et al. 2009), and these compounds have been found in many plants including maize, wheat, and rye (*Secale cereale*) (Frey et al. 2009). The benzoxazinoid biosynthetic pathway is well-characterized in maize (Supplemental Fig. S10A). Metabolic profiling previously revealed that levels of both DIBOA-glucoside (DIBOA-Glc) and DIMBOA-glucoside (DIMBOA-Glc), the storage forms of DIBOA and DIMBOA, were markedly lower in maize lines tolerant to Pi limitation, which are able to take up Pi more efficiently under low Pi conditions (Luo et al. 2019). In our present study, we determined that *Bx* genes (*Bx1-Bx9*)

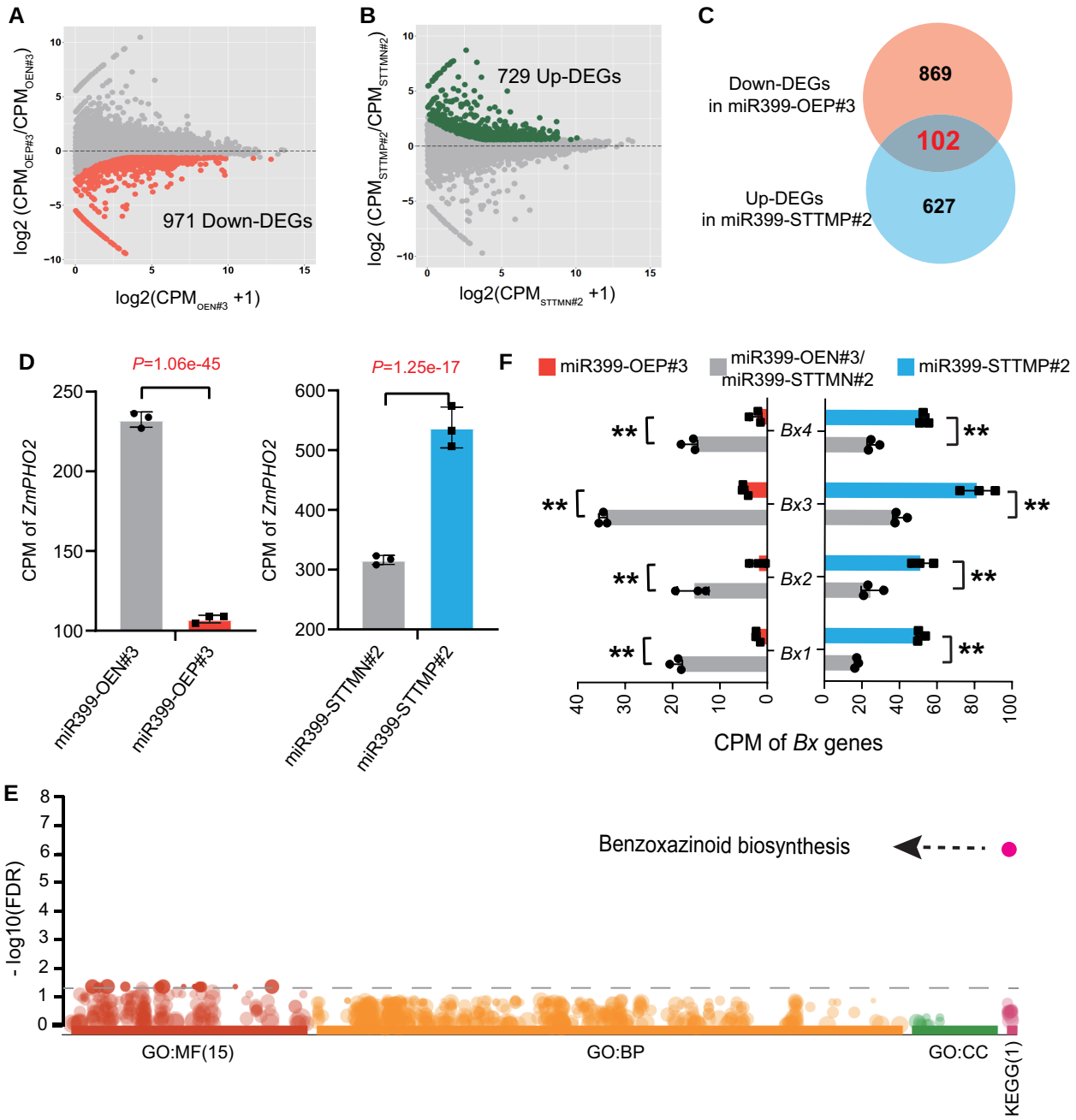

Figure 3. RNA-seq analysis reveals that miR399 might mediate pathogen and insect resistance in maize, in addition to affecting Pi responses. **A)** Differentially expressed genes (DEGs) in the miR399-OE transgene-positive line (miR399-OEP#3) compared with its transgene-negative line (miR399-OEN#3). A total of 971 downregulated genes (down DEGs) were detected in miR399-OEP#3. **B)** DEGs in the miR399-STTM transgene-positive line (miR399-STTMP#2) compared with its transgene-negative line (miR399-STTMN#2). A total of 729 upregulated genes (up DEGs) were detected in miR399-STTMN#2. **C)** Overlap of the downregulated DEGs in miR399-OEP#3 and upregulated DEGs in miR399-STTMP#2. **D)** *ZmPHO2* expression in miR399-OE and miR399-STTM transgene-positive lines (miR399-OEP#3 and miR399-STTMP#2) and their corresponding transgene-negative lines (miR399-OEN#3 and miR399-STTMN#2). *P*-values were calculated by DESeq2 after multiple correction of the FDR. **E)** Gene ontology (GO) and KEGG pathway enrichment analyses of the 102 overlapping DEGs. Benzoxazinoid biosynthesis was the most highly enriched pathway. BP, biological process; MF, molecular function; CC, cellular component groups of GO. The total number of enriched categories in the GO or KEGG group is indicated in parentheses. **F)** Expression of several key *Bx* genes (*Bx1* to *Bx4*) in the benzoxazinoid biosynthesis pathway in the miR399-OE and miR399-STTM transgene-positive lines and their corresponding transgene-negative lines. $^{**}P \leq 0.01$.

involved in benzoxazinoid biosynthesis are significantly downregulated in miR399-OE transgene-positive lines, as shown by the RNA-seq data and RT-qPCR validation (Fig. 3F; Supplemental Figs. S11, B and S12), which should result in a reduced accumulation of benzoxazinoid compounds. To test this idea, we performed a targeted

high-performance liquid chromatography (HPLC) assay with DIBOA and DIMBOA as standards. We measured significantly lower levels of both DIBOA and DIMBOA in miR399-OE plants, thus validating our hypothesis (Supplemental Fig. S13A). By contrast, the expression levels of most *Bx* genes tended to be upregulated and the metabolites (DIBOA and DIMBOA) accumulated to higher levels in miR399-STTM plants (Fig. 3F; Supplemental Figs. S12 and S13B). Collectively, these results support the conclusion that miR399 might influence pathogen and insect defense in maize, in addition to its effects on the Pi response and leaf senescence. However, how the expression of *Bx* genes is modulated in miR399-OE or miR399-STTM transgenic lines is still an open question. A similar scenario was noted in rice, where Pi accumulation induced by overexpressing *OsMIR399f* or high levels of Pi fertilization resulted in enhanced susceptibility to infection by the blast fungus *Magnaporthe oryzae* (Campos-Soriano et al. 2020), demonstrating that miR399 functions as a negative regulator of plant immunity, possibly through an indirect mechanism.

Mutation of *ID1* promotes miR399 expression and facilitates Pi accumulation in maize

ID1 is a monocotyledon-specific zinc-finger transcription factor that plays an essential role in regulating the transition to flowering in maize. Loss-of-function *id1* mutants experience a prolonged period of vegetative growth causing an extreme delay in flowering, ultimately resulting in vegetative gigantism (Singleton 1946; Colasanti et al. 1998; Colasanti and Sundaresan 2000). Although the *id1* mutation severely alters the ability of maize to undergo the transition to reproductive growth, homozygous *id1* plants are virtually identical in growth rate and morphology to wild-type maize plants until the point of floral transition (Singleton 1946; Colasanti et al. 1998; Coneva et al. 2007). Transcriptome profiling revealed that miR399 accumulated to abnormally high levels in both mature and immature leaves of the *id1-m1* mutant at the floral transition stage (Minow et al. 2018). By reanalyzing the small RNA-seq data from this earlier study (Minow et al. 2018), we confirmed that members of the miR399 family (including miR399a/c/h, miR399e/i/j, miR399b, and miR399f) are significantly more abundant in mature leaves of the *id1-m1* mutant (Fig. 4A; Supplemental Fig. S14). In immature leaves, miR399e/i/j also accumulated to higher levels in the *id1-m1* mutant than in the wild type (Supplemental Fig. S14), while other members were slightly more abundant or unchanged. Using the corresponding RNA-seq data (Minow et al. 2018), we established that *ZmPHO2* transcript levels are significantly downregulated in the *id1-m1* mutant (Supplemental Fig. S15). Considering the nutritional requirements for vigorous vegetative growth and extremely delayed flowering, we speculated that the upregulation of miR399 in the *id1* mutant might help provide more Pi to sustain the extra vegetative growth of this mutant. This hypothesis prompted us to examine the relationship between ID1 and the miR399-*ZmPHO2* regulatory module.

To independently confirm the small RNA-seq results, we created a new *id1* mutant by CRISPR/Cas9-mediated gene editing and obtained an edited plant with a large deletion in the *ID1* coding region (Supplemental Fig. S16A). Genotyping and sequencing of the targeted genomic region in T2 populations derived from 1 T1 heterozygous mutant allowed the identification of 1 homozygous mutant without the *Cas9* transgene. The homozygous mutant, which was named *id1-c1*, showed lower expression of *ID1* (Supplemental Fig. S16B) and vigorous vegetative growth and extremely delayed flowering in the field reminiscent of the original *id1-m1* mutant (Supplemental Fig. S16, C and D). These molecular and phenotypic characteristics indicated that we had successfully obtained an *id1* mutant by gene editing. RNA gel blot analysis confirmed that miR399 levels are significantly increased in mature and immature leaves at the floral transition stage of the *id1-c1* mutant (Fig. 4B). In addition, consistent with the reported RNA-seq data (Supplemental Fig. S15) (Minow et al. 2018), we confirmed that *ZmPHO2* expression is significantly downregulated in the *id1-c1* mutant relative to the wild type (i.e. the corresponding transgene-free and editing-free sibling) by RT-qPCR (Fig. 4C).

We examined *ID1* expression in miR399-OE and miR399-STTM transgenic lines by RNA-seq and RT-qPCR but did not detect a significant difference compared with the wild type (Fig. 4D; Supplemental Fig. S17), which supports the notion that *ID1* is genetically upstream of the miR399-*ZmPHO2* module. We also measured the total phosphorus content of the *id1-c1* mutant at the floral transition stage and detected 2-fold higher phosphorus levels in mature leaves compared with the wild type (Fig. 4E). In other tissues, including immature leaves, roots, leaf sheaths, and stems, we observed no significant changes in phosphorus content (Supplemental Fig. S18). Altogether, these observations show that loss of ID1 function facilitates Pi accumulation in mature leaves, perhaps via the miR399-*ZmPHO2* regulatory module. Increased Pi accumulation might provide an adequate nutritional reserve for the vigorous vegetative growth of the *id1* mutant.

ID1 directly binds to the promoters of *ZmMIR399c* and *ZmMIR399j* to repress their transcription

We determined the levels of the primary transcripts (pri-miR399s) derived from the *ZmMIR399a*, *ZmMIR399c*, *ZmMIR399h*, *ZmMIR399e*, *ZmMIR399i*, and *ZmMIR399j* loci, which are responsible for the production of miR399a/c/h and miR399e/i/j. We determined that, in both mature and immature leaves of the *id1-c1* mutant, *ZmMIR399c* and *ZmMIR399j* levels are markedly upregulated, while the expression of other *ZmMIR399* genes was slightly upregulated or unchanged (Fig. 5A), indicating that the enhanced accumulation of miR399a/c/h and miR399e/i/j in the *id1-c1* mutant was mainly due to *ZmMIR399c* and *ZmMIR399j* expression, respectively. We examined whether ID1 might regulate the transcription of *ZmMIR399c* and *ZmMIR399j*

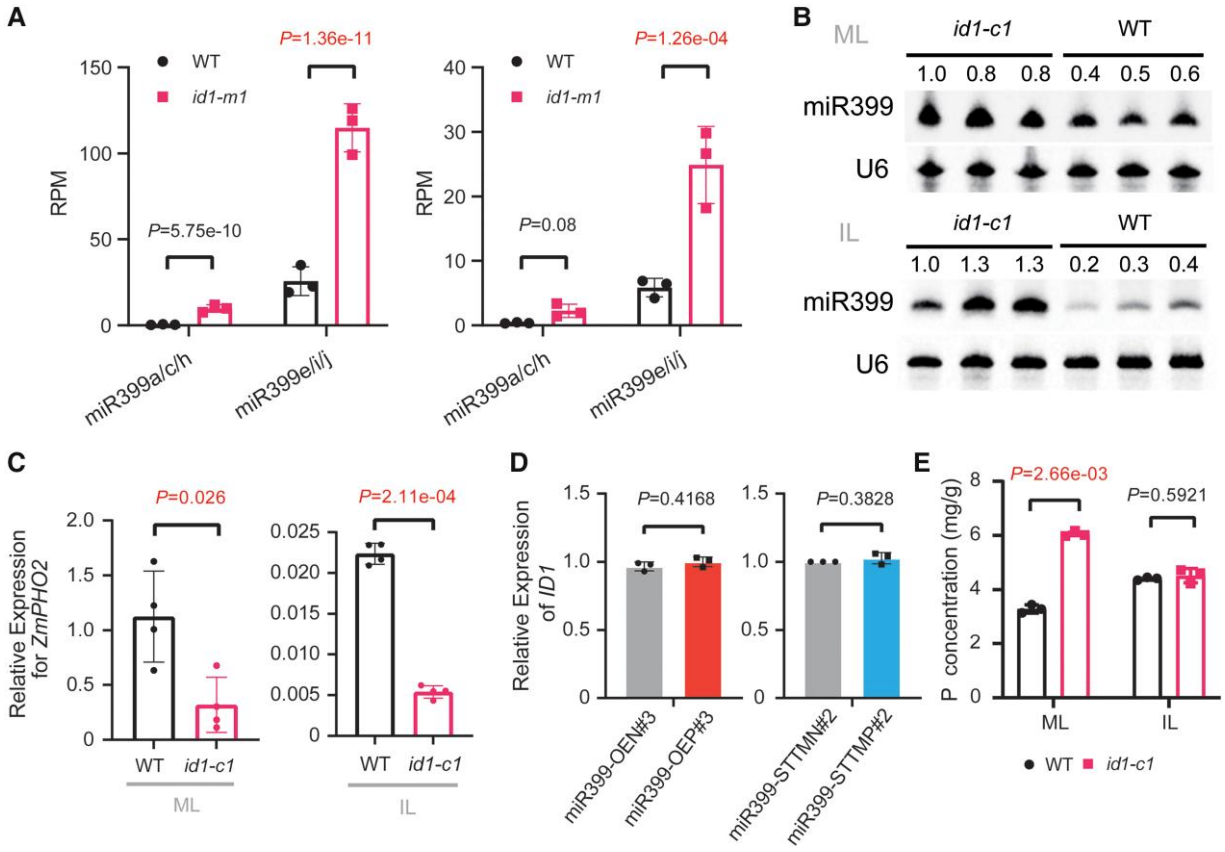

Figure 4. Mutation of *ID1* promotes miR399 accumulation and facilitates Pi accumulation in maize. **A)** Abundance of miR399a/c/h and miR399e/i/j in the *id1-m1* mutant and wild type (WT) based on small RNA-seq data (Minow et al. 2018). The left and right panels represent results of small RNA-seq in mature leaves and immature leaves, respectively. RPM, reads per million. Values are means ± SD. *P*-values were calculated by DESeq2 after multiple correction of the FDR. **B)** RNA gel blot detection of miR399 in mature leaves (ML) and immature leaves (IL) of the *id1-c1* mutant and the wild type (WT). U6 served as an internal control. The numbers indicate the abundance of miR399 relative to the first lane. **C)** *ZmPHO2* expression in mature leaves (ML) and immature leaves (IL) of WT and the *id1-c1* mutant ($n = 3$), as determined by RT-qPCR. *ZmPHO2* expression was normalized to that of *ZmUBI*. **D)** *ID1* expression levels in miR399-OE (OE#3) transgenic lines and miR399-STTM (STTM#2) transgenic lines ($n = 3$). *ID1* expression was normalized to that of *ZmUBI*. **E)** Total phosphorus (P) content in mature leaves (ML) and immature leaves (IL) of the *id1-c1* mutant and wild type (WT) at the floral transition stage. The values in panels **C)** to **E)** are means ± SD. Student's *t*-test (Supplemental Data Set S6) was employed to calculate the *P*-values.

via a dual-LUC reporter assay, using the coding sequence of *ID1* driven by the 35S promoter (*p35S:ID1*) as the effector and *LUC* driven by either the *ZmMIR399c* or the *ZmMIR399j* promoter (*proMIR399c:LUC and proMIR399j:LUC*), as the reporter (Fig. 5B). We observed that the LUC activity derived from the *proMIR399c:LUC* and *proMIR399j:LUC* reporter constructs is significantly repressed in maize protoplasts when the *p35S:ID1* effector was cotransfected (Fig. 5B).

The transcription factor ID1 was previously shown to selectively bind to an 11-bp consensus element by in vitro DNA selection and amplification-binding assays and DNA-binding experiments (Kozaki et al. 2004). Transient expression of a construct encoding a fusion between ID1 and the green fluorescent protein (ID1-GFP) in *Nicotiana benthamiana* leaves showed that ID1 mainly localizes in the nucleoplasm (Supplemental Fig. S19), in line with its potential role as a transcription factor. Sequence analysis of the 2-kb regions upstream of the annotated 5′ ends of *ZmMIR399c* and *ZmMIR399j* revealed 6 and 2 copies, respectively, of a typical ID1-binding motif (Fig. 5C; Supplemental Fig. S20). To assess whether ID1 can bind directly to these promoter regions, we purified a recombinant maltose-binding protein-tagged version of ID1 (MBP-ID1) in *Escherichia coli* (Supplemental Fig. S21) and performed electrophoretic mobility shift assays (EMSA) and in vitro DNA pull-down experiments by incubating biotin-labeled probes with recombinant MBP-ID1. We determined that ID1 binds to DNA fragments containing the motifs, while the corresponding nonbiotin-labeled competitors neutralized this binding activity (Fig. 5, C and D). Mutation of the motif completely abolished ID1 binding (Fig. 5, C and D). We also utilized a *35S:ID1-3×HA* transgenic line (Supplemental Fig. S22) to conduct a chromatin immunoprecipitation (ChIP) experiment in leaf tissue. Immunoprecipitation with an anti-HA antibody

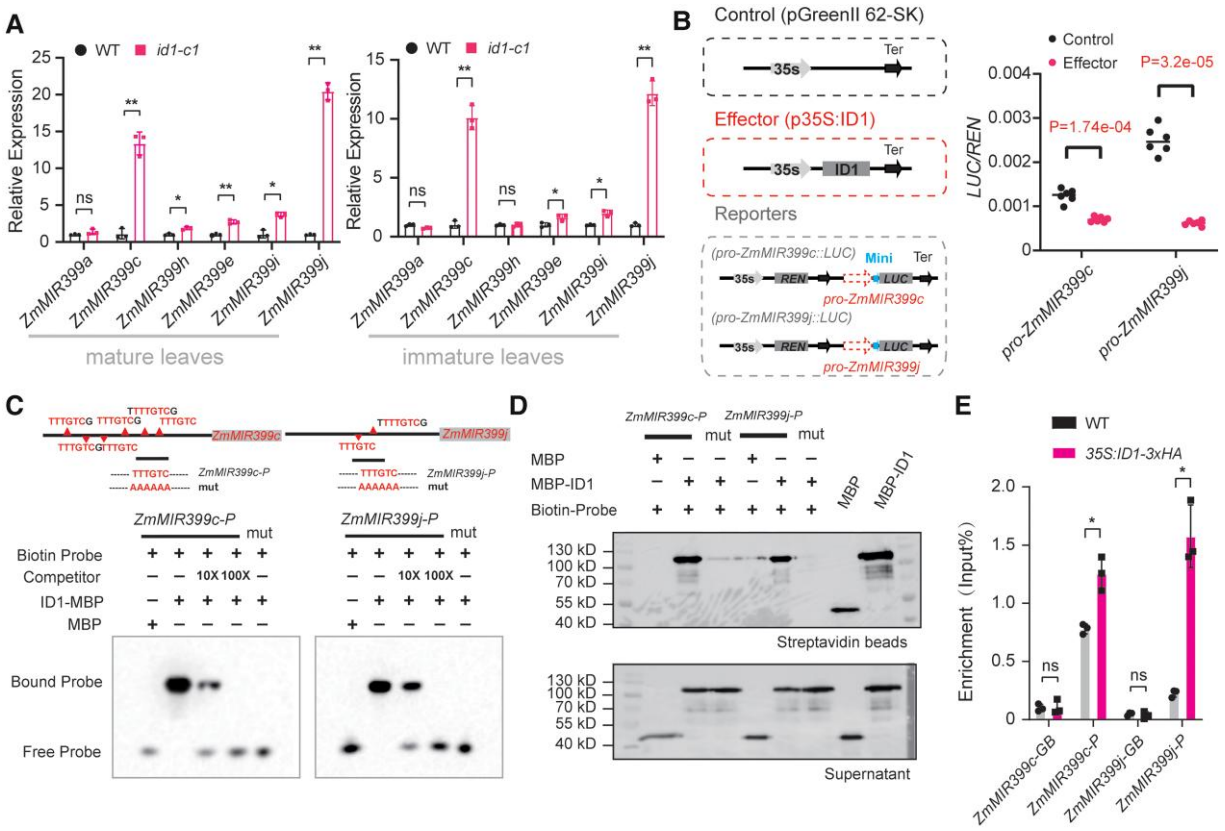

Figure 5. ID1 functions as an upstream regulator by binding directly to the promoter regions of *ZmMIR399c* and *ZmMIR399j*. **A)** Expression levels of 6 primary miR399 precursors (*ZmMIR399a, c, h, e, i, j*) in mature leaves and immature leaves of the *id1-c1* mutant and wild type (WT) by RT-qPCR. Expression levels were normalized to that of *ZmUBI*. Values are means ± SD; the *P*-values were determined by Student's *t*-test (Supplemental Data Set S6). **B)** Schematic diagram showing the effector and reporter constructs used in the transient transcription activity assays. *REN*, Renilla luciferase; *LUC*, firefly luciferase; Mini: minimal 35S promoter. Values means ± SD based on the technical replicates ($n = 6$) of 1 representative out of 3 independent experiments; Student's *t*-test (Supplemental Data Set S6) was used to calculate the *P*-values. **C)** EMSA showing the binding of ID1 to the *ZmMIR399c* and *ZmMIR399j* promoters. Top, distribution of predicted ID1-binding motifs in the *ZmMIR399c* and *ZmMIR399j* promoter. The black lines indicate the biotin-labeled probes (*ZmMIR399c*-P and *ZmMIR399j*-P) used in EMSA and in vitro DNA pull-down experiments. Bottom, EMSAs showing binding of ID1 protein to the predicted motifs in the *ZmMIR399c* and *ZmMIR399j* promoters. "mut" represents biotin probes with the binding motif mutated (Supplemental Data Set S5). **D)** DNA pull-down analysis showing the binding of ID1 to *ZmMIR399c* and *ZmMIR399j* promoters at the predicted motifs. Biotin-labeled probes, *ZmMIR399c*-P and *ZmMIR399j*-P, were used to pull down recombinant MBP (control) and MBP-ID1, which were then detected by immunoblotting using an anti-MBP antibody in both the beads and the supernatant. **E)** Chromatin immunoprecipitation (ChIP) showing the association of ID1 with the *ZmMIR399c* and *ZmMIR399j* promoters in vivo. Chromatin from the leaves of *35S:ID1-3×HA* transgenic or wild-type (WT) plants was immunoprecipitated with anti-HA Trap. The enrichment (IP%) of the 2 promoter fragments (*ZmMIR399c*-P and *ZmMIR399j*-P shown in **C**) was determined by qPCR. Asterisks indicate significant difference between the *35S:ID1-3×HA* transgenic line and wild type (WT) (*$P \leq 0.05$; Student's *t*-test, Supplemental Data Set S6). The gene body regions of *ZmMIR399c* and *ZmMIR399j* (*ZmMIR399c*-GB and *ZmMIR399j*-GB) were used as negative controls.

detected a specific enrichment of ID1-3×HA at the promoter regions of *ZmMIR399c* and *ZmMIR399j* that encompass the probe sequences (Fig. 5, C and E). Taken together, these results demonstrate that ID1 directly binds to the promoter regions of *ZmMIR399c* and *ZmMIR399j* and represses their transcription.

We further investigated the response of *ID1* expression to low-Pi stress by growing the maize inbred line B73 in hydroponic solution containing normal Pi (NP; 250 μM KH_2PO_4) or low Pi (LP; 5 μM KH_2PO_4). We imposed low-Pi treatment for 3 d or 5 d prior to the reproductive transition stage when *ID1* is specifically expressed. Mature and immature leaves were collected and used for total RNA isolation and expression analysis at the floral transition stage. We first confirmed that the abundance of Pi-responsive miR399 and the long noncoding RNA *PILNCR1* is elevated under low-Pi conditions (Supplemental Fig. S23), indicating the efficacy of treatment in the hydroponic system in imposing quantitative Pi stress on the plants. However, we did not detect expression changes for *ID1* under low-Pi conditions (Supplemental Fig. S24), indicating that ID1 is not Pi responsive, but rather an autonomous regulator in maize.

Based on all the above observations, we propose that loss of ID1 function triggers the miR399-*ZmPHO2* pathway, which

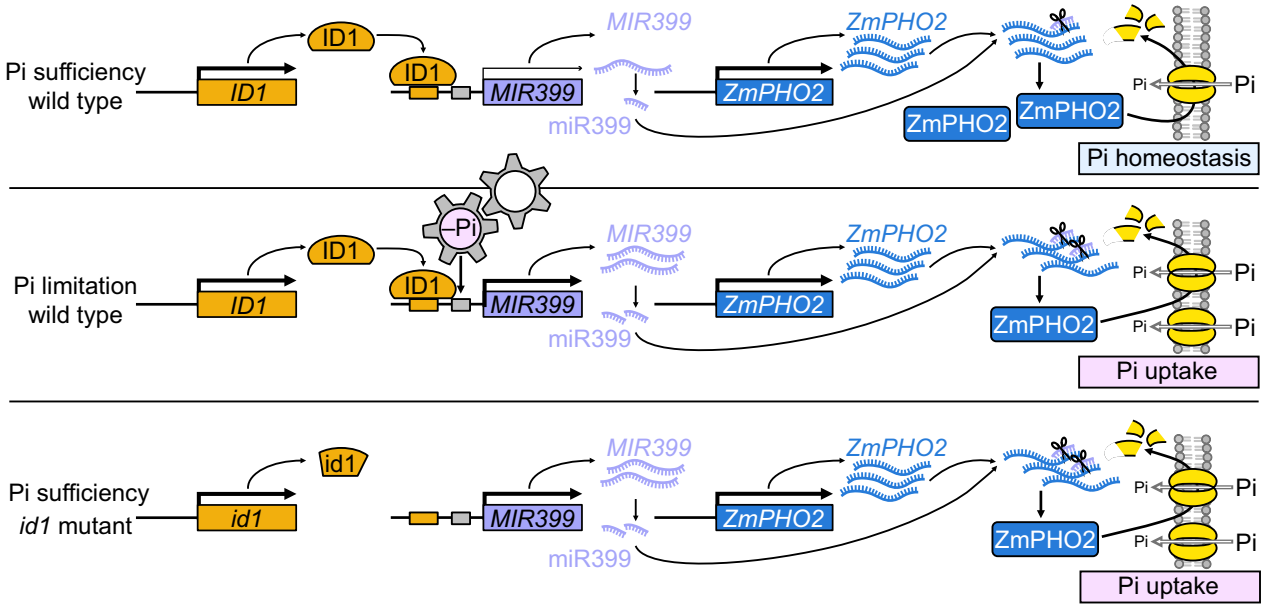

Figure 6. Proposed model for the function of *ID1* as a Pi homeostasis regulator. In the absence of Pi stress (upper panel), ID1 represses the expression of *ZmMIR399* genes to maintain in vivo Pi homeostasis and normal metabolism. Under Pi limitation (middle panel), the expression of *ID1* is not responsive. However, *ZmMIR399* expression can be directly upregulated by the response of Pi limitation, which finally promotes Pi uptake through downregulating *ZmPHO2*. When ID1 is mutated (lower panel), derepression of *ZmMIR399* promotes the accumulation of mature miR399, with elevated miR399 levels knocking down the expression of *ZmPHO2*, resulting in enhanced Pi acquisition and transport. The size of the black arrows indicates expression levels.

enhances Pi acquisition and transport, and finally leads to higher Pi levels that are able to support the vegetative gigantism of the *id1* mutant (Fig. 6). This situation contrasts with that of wild-type plants, where ID1 lowers miR399 levels by repressing the transcription of *ZmMIR399c* and *ZmMIR399j*, which in turn maintains Pi homeostasis (Fig. 6), underscoring ID1 as an autonomous Pi regulator upstream of the miR399-*ZmPHO2* signaling pathway.

ZmPHO2 was under selection during maize domestication

Crop domestication has not only been shaped by artificial selection but also by natural selective pressures (Martín-Robles et al. 2019). Natural selection under modern agricultural conditions, which differ from wild habitats in the availability of resources, might have led to changes in crops for both their external morphology and internal metabolism. Cultivated maize originated in the tropical environment of southwestern Mexico and has since spread widely to temperate zones having topsoil properties that differ from those of tropical areas. In tropical and subtropical regions, such as the Cerrado region in Brazil, acidic soils with low Pi availability are prevalent (Goedert 1983; Aguirre-Liguori et al. 2019). Under these conditions, without human intervention, the ancestral maize may have needed a more efficient Pi uptake system to ensure its survival. In humid temperate regions, Pi is more concentrated at the surface, a considerable portion being in the form of organic compounds (Lynch and Brown 2001). Under these conditions, cultivated maize can have better access to Pi. Furthermore, the use of fertilizer, which tends to be overapplied by farmers to guarantee adequate levels of crop yield and quality, makes Pi easily available. Thus, both natural and artificial selection pressures might have promoted changes in the Pi uptake/transport system during domestication or postdomestication dispersal of maize. We speculated that *ZmPHO2*, as a major Pi regulator, might have been targeted by selection as maize became domesticated and spread to temperate zones.

To test this hypothesis, we first analyzed the nucleotide diversity around ten *ZmMIR399* genes and *ZmPHO2* using the third-generation *Z. mays* haplotype map (HapMap 3), which includes ultrahigh-density single nucleotide polymorphism (SNP) data for various maize and teosinte accessions (Bukowski et al. 2018). We observed that the regions around *ZmMIR399c* and *ZmMIR399j* show a slight decrease in nucleotide diversity in maize and landraces compared with the teosinte group (Supplemental Fig. S25). Notably, the 5′ UTR of *ZmPHO2*, in which the miR399-binding sites are located, exhibited a clear drop in nucleotide diversity in maize compared with landraces or teosinte, with the maize group retaining only 29% of the genetic diversity of the teosinte group (Fig. 7A). We confirmed this observation by resequencing a ∼1.6-kb 5′ UTR fragment in 26 diverse maize inbred lines and 14 teosinte accessions (*Z. mays* ssp. *parviglumis*) (Supplemental Table S1). On average, we determined that maize ($\pi = 0.00266$) retained 33.7% of the nucleotide diversity of teosinte ($\pi = 0.00788$; Fig. 7B), with 2 specific regions (∼1.2 kb and ∼400 bp upstream of the ATG) showing very

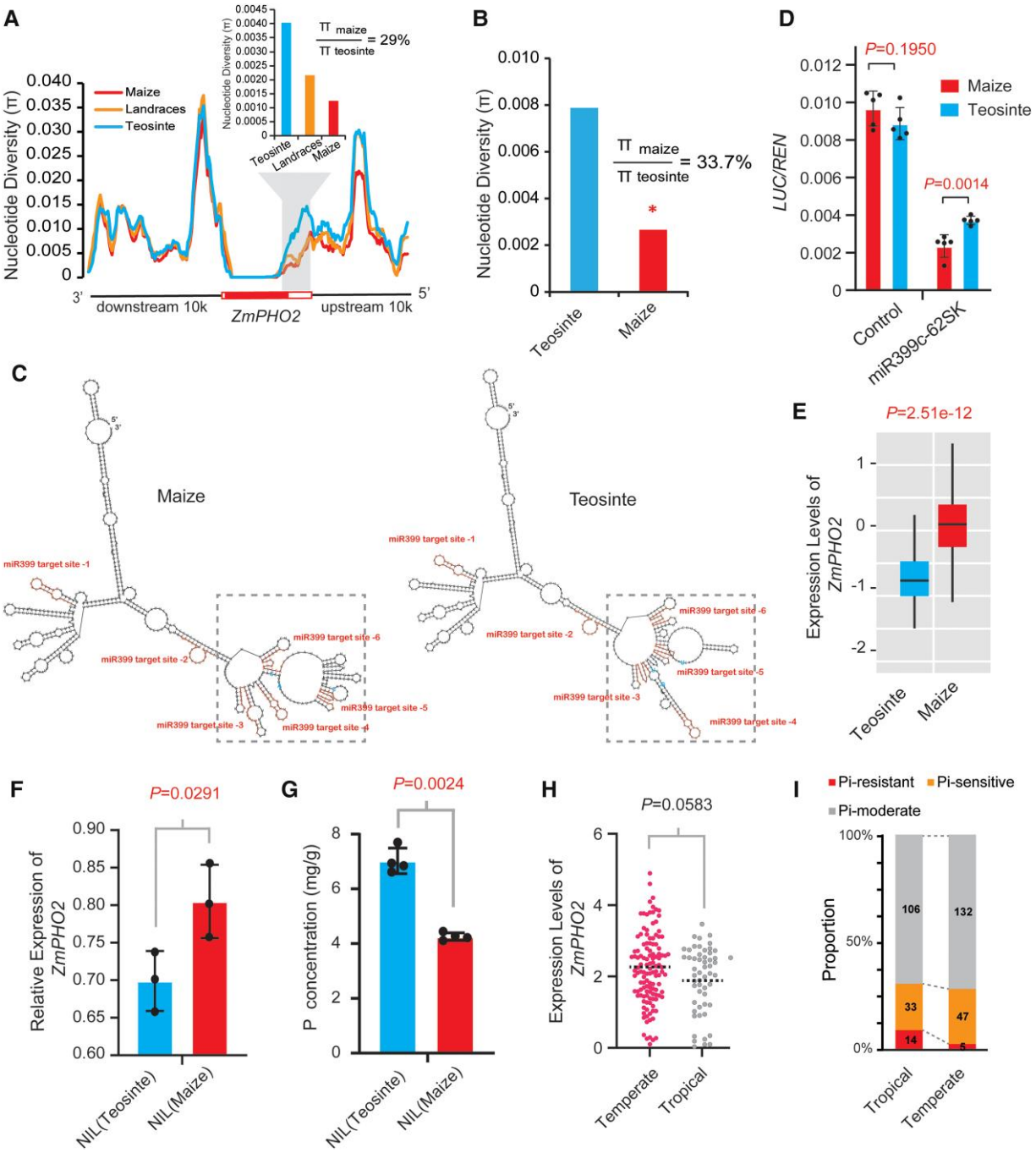

Figure 7. Evidence of selection at *ZmPHO2*. **A)** The 5′ regulatory region of *ZmPHO2* exhibits low nucleotide diversity (π) in maize relative to teosinte, as analyzed with the maize HapMap v3 SNP data. The nucleotide diversity of maize, teosinte, and landraces is shown with red, blue, and orange lines or bars, respectively. White and red rectangles in the gene structure of *ZmPHO2* under the line plot indicate the UTR and coding regions, respectively. **B)** Resequencing data for 26 maize inbreds and 14 teosinte accessions indicating that maize retained an average of the 33.7% nucleotide diversity seen in teosinte in the resequenced 5′ UTR. *$P < 0.05$ from the coalescent simulations. **C)** RNA secondary structures predicted by the RNAfold WebServer. The region from 100 bp upstream of the first miR399-binding site to 100 bp downstream of the 6th miR399-binding site of representative maize and teosinte lines was used for structure prediction. Red, miR399-binding sites; blue, conserved SNPs between maize and teosinte. **D)** Transient coexpression assays in maize protoplasts using *miR399c* as the effector and *ZmPHO2* 5′ UTR^{maize}:*LUC* and *ZmPHO2* 5′ $UTR^{teosinte}$:*LUC* as reporters. Values are means ± SD based on the technical replicates ($n = 5$); two-tailed Student's *t*-test was used to calculate the *P*-values (Supplemental Data Set S6). **E)** *ZmPHO2* expression levels in maize and teosinte, based on data from Wang et al. (2018). **F)** *ZmPHO2* expression levels in *ZmPHO2-NIL*^{maize} and *ZmPHO2-NIL*^{teosinte} as examined by RT-qPCR, normalized to that of *ZmUBI*. Values are means ± SD. Student's *t*-test (Supplemental Data Set S6) was employed to calculate the *P*-value. **G)** Total phosphorus (P) content in *ZmPHO2-NIL*^{maize} and *ZmPHO2-NIL*^{teosinte}. Values are means ± SD. Student's *t*-test (Supplemental Data Set S6) was employed to calculate the *P*-value. **H)** *ZmPHO2* expression levels in the root tissues of tropical and temperate inbred maize lines, based on data from (Kremling et al. 2018). *P*-values were calculated by a Kolmogorov–Smirnov test (Supplemental Data Set S6). **I)** Proportion of Pi-tolerant, Pi-sensitive, and Pi-moderate lines in tropical and temperate maize groups. The data are from (Luo et al. 2019).

low nucleotide diversity in maize relative to teosinte (Supplemental Fig. S26). Coalescent simulations that incorporate the domestication bottleneck (Eyre-Walker et al. 1998; Tian et al. 2009) detected a significant deviation from expectation under a neutral domestication bottleneck for this resequenced region ($P < 0.5$; Fig. 7B), indicating that the 5′ UTR of *ZmPHO2* was affected by selection. Although the miR399-binding sites do not show any sequence differences among the resequenced maize and teosinte accessions, we detected SNPs around the miR399-binding sites, which might affect the accessibility of miR399 and thus alter *ZmPHO2* transcript levels. To test this hypothesis, we first predicted RNA secondary structures of a 5′ UTR fragment containing the miR399-binding sites (including 100 bp upstream of the first binding site and 100 bp downstream of the 6th binding site) with representative maize and teosinte sequences. Three conserved SNPs between maize and teosinte were present in this region and were predicted to affect the RNA secondary structures (Fig. 7C). Thus, it is possible that the SNPs affect the ability of miR399 to access its binding sites. To test whether the SNPs affect the activity of miR399, we performed transient coexpression assays in maize protoplasts using the minimal 35S promoter driving a 1.6-kb partial 5′ UTR fragment of *ZmPHO2* (indicated by the magenta line segment in Fig. 2A) from maize and teosinte cloned upstream of *LUC* as reporters; we selected the miR399c precursor as a representative that we cloned as effector (see details in Materials and Methods). We observed that overexpression of the miR399c precursor effectively reduced LUC activity in both the maize and teosinte 5′ UTR reporters (Fig. 7D), which is consistent with the negative regulatory role of miR399 on *ZmPHO2*. Interestingly, miR399c showed higher inhibition of LUC activity derived from the maize 5′ UTR fragment than that of teosinte (Fig. 7D), suggesting that the 3 SNPs around the miR399-binding sites do affect the accessibility of miR399 to its binding sites in the 5′ UTR. The stronger repression in the maize 5′ UTR context may result in lower expression of *ZmPHO2* in maize compared with teosinte; however, other regulatory elements may also affect *ZmPHO2* expression.

To holistically examine the potential *cis*-regulatory effects on *ZmPHO2* expression caused by maize and teosinte sequence divergence, we searched for *cis*-eQTL (expression quantitative trait locus) at *ZmPHO2* using a maize–teosinte recombinant inbred line (RIL) population (Wang et al. 2018). We detected a strong *cis*-eQTL for *ZmPHO2*, with the maize allele showing a significantly higher expression level than the teosinte allele (Fig. 7E). To validate the effects of this *cis*-eQTL on *ZmPHO2* expression, we developed a pair of near-isogenic lines (NILs) across the *ZmPHO2* region from the same RIL population: the expression of *ZmPHO2* was significantly higher in *ZmPHO2*-NIL^{maize} harboring the maize allele of *ZmPHO2* than in *ZmPHO2*-NIL^{teosinte} carrying the teosinte allele in an otherwise homogeneous maize (W22 inbred line) background (Fig. 7F). Thus, the *cis*-eQTL likely contains positive elements outside of the ∼1.6-kb 5′ UTR fragment used for the transient coexpression assay that enhance *ZmPHO2* expression in maize such that the negative effects of the SNPs near the miR399-binding sites are overridden. However, the limited resolution of the *cis*-eQTL prevented us from pinpointing the position of such positive elements. In agreement with a role for *ZmPHO2* as a negative regulator of Pi uptake, *ZmPHO2*-NIL^{maize} lines exhibited a significantly lower total Pi level than *ZmPHO2*-NIL^{teosinte} lines (Fig. 7G). These results indicate that *ZmPHO2* may have been a target of selection during maize domestication, leading to weaker Pi uptake in cultivated maize. We further examined the difference in expression of *ZmPHO2* between temperate and tropical maize inbred lines using published RNA-seq data of a maize association panel (Kremling et al. 2018). This analysis revealed that the temperate lines tend to have higher *ZmPHO2* expression levels than tropical lines in root tissues (Fig. 7H), suggesting that adapting maize from tropical regions to temperate zones was associated with an expression divergence of *ZmPHO2*. In addition, a recent study evaluated low-Pi tolerance in another maize association panel, which also included different sources of maize inbred lines (Fang and Luo 2019). Using the classification criteria of that study, we noticed a greater percentage of low-Pi-sensitive lines and a lower percentage of low-Pi-tolerant lines in the temperate maize subgroup than in the tropical maize subgroup (Fig. 7I), indicating that the temperate maize inbreds are more sensitive to low-Pi stress. Combined with the higher expression of *ZmPHO2* in temperate maize relative to tropical maize, these observations suggest that Pi uptake ability might have degenerated as maize spread into temperate zones with high Pi cultivation environments from original tropical habitats. Taken together, the above results suggest that *ZmPHO2* expression was affected by domestication or subsequent cultivation and may therefore have mediated the change of Pi uptake system during maize cultivation.

Discussion

Maize yield is largely limited by Pi poor availability in most cropping soils worldwide. Therefore, application of phosphorus fertilizers to cultivated crop plants is essential to ensure high-yielding agriculture. Given that global phosphorus resources are finite and rapidly diminishing, identifying Pi homeostasis regulators and dissecting the regulatory mechanism of Pi homeostasis are fundamental for developing Pi-efficient cultivars. In this study, we report that ID1, previously known as a floral transition regulator, can directly bind to the promoters of *ZmMIR399* genes to inhibit their transcription, thus reducing the accumulation of mature miR399 and alleviating the repression of *ZmPHO2* imposed by miR399. We conclude that *ID1*-miR399-*ZmPHO2* contributes to the maintenance of Pi homeostasis in maize as a regulatory module. Interestingly, *ID1* expression was independent of external Pi limitation, suggesting that ID1 is an autonomous regulator of Pi homeostasis. Our study revealed a direct functional link between Pi-limitation sensing by the miR399-*ZmPHO2* regulatory module and plant

developmental regulation by ID1, although further understanding of whether ID1 is integrated with other Pi regulators is still needed. Importantly, we also established that *ZmPHO2* was under selection during maize domestication and cultivation, resulting in more sensitivity to Pi limitation in temperate maize than in tropical maize. We speculate that the degeneration of nutrient uptake ability might be a common phenomenon as maize spread to temperate zones with adequate soil nutrients.

ID1, as an upstream repressor, might regulate the miR399-*ZmPHO2* module independently of known regulators

Several regulators involved in maintaining Pi homeostasis have been identified in plants (Rubio et al. 2001; Bari et al. 2006; Chen et al. 2007; Devaiah et al. 2007b; Zhou et al. 2008; Devaiah et al. 2009; Wang et al. 2013b). AtPHR1, a MYB-type transcription factor, was the first regulator demonstrated to mediate the Pi-starvation response; it plays a central role in transcriptional regulation of a large subset of Pi limitation-responsive genes, including *ZmMIR399* (Bari et al. 2006). In the promoter regions of *ZmMIR399* genes, AtPHR1 binds to the predicted PHR1-specific binding sequence (P1BS), resulting in positive regulation of miR399 accumulation. In a similar manner, PHR1 orthologs have been reported to act as transcription factors upstream of the miR399-*PHO2* regulatory module in several plant species, including maize, rice, and wheat (Zhou et al. 2008; Wang et al. 2013a; Wang et al. 2013b). In maize, overexpression of *ZmPHR1* significantly increases Pi content in shoots under low-Pi conditions (Wang et al. 2013b). By investigating the change in expression of *ZmPHR1* and its closest ortholog, *ZmMYB78*, we determined that both genes show similar transcript levels in immature leaves and mature leaves, and between the *id1-c1* mutant and wild-type plants (Supplemental Fig. S27), suggesting that *ZmPHR1* and *ZmMYB78* are not genetically downstream of *ID1*. *PILNCR*, a Pi deficiency-induced long noncoding RNA previously identified in maize, regulates the function of miR399 by competitively binding and sequestering the miRNA (Du et al. 2018). We also assessed the expression of *PILNCR* by RT-qPCR and measured similar expression levels in both the *id1-c1* mutant and wild type (Supplemental Fig. S27). Combined with the experimental evidence showing the binding of ID1 to *ZmMIR399* promoters, these expression results support the notion that ID1 is a direct upstream regulator of *ZmMIR399* transcription. It is possible that ID1 regulates the miR399-*ZmPHO2* module independently of *ZmPHR1*.

ID1 controls Pi homeostasis, likely through systemic movement of miR399, in maize and possibly other crops

Plants take up mineral nutrients from the rhizosphere via roots and the nutrients are subsequently distributed to aboveground shoots. The demand by shoots for nutrients and their supply from roots need to be properly coordinated to maintain the normal growth and development of plants. Long-distance signaling pathways can be triggered by internal or external factors as a component of adaptive responses when the nutrient status in shoots fluctuates (Forde 2002; Atkins and Smith 2007, 2007). Thus, when a change in internal nutrient status in shoots is sensed, this information is transduced by long-distance signals to roots, which ensures the integration of nutritional demands in shoots with physiological changes in roots. Many nutrient uptake systems involved in nutrient assimilation and mobilization in roots are regulated by demand from the shoot via shoot-derived signals (Marschner 1995).

In Arabidopsis, miR399 generated in shoots serves as a long-distance signal that represses *PHO2* expression in roots under Pi limitation conditions, resulting in the activation of Pi uptake and translocation (Lin et al. 2008; Pant et al. 2008). In maize, *ZmPHO2* transcripts in roots can be knocked down by miR399, whose precursor *MIR399* is expressed in the vascular systems, ultimately leading to Pi overaccumulation in shoots (Du et al. 2018). In the present study, we also found that more Pi accumulated in shoots of miR399-overexpressing transgenic maize than in the wild type (Fig. 1B), in line with observations in Arabidopsis (Lin et al. 2008). However, in our miR399-OE transgenic maize, it is not clear whether miR399 is transported to roots to enhance Pi uptake there, because of the constitutive accumulation of mature miR399. In Arabidopsis, *N. benthamiana*, and soybean, micrografting experiments have been employed to determine the shoot-to-root movement of mature miRNAs (Pant et al. 2008; Kasai et al. 2010; Huen et al. 2018; Li et al. 2021). However, it is still very challenging to perform micrografting in maize, although a recent breakthrough was reported showing that the embryonic hypocotyl allows grafting in most monocotyledonous orders (Reeves et al. 2022). Accordingly, it might soon be possible to investigate the shoot-to-root movement of miR399 in maize as well.

The spatial patterns of *ID1* expression led us to speculate that its role in regulating Pi homeostasis involves mobile miR399. *ID1* is expressed exclusively in developing leaves (Colasanti et al. 1998), where it is expected to repress the expression of *ZmMIR399* genes. In *id1* mutants, the repression of *ZmMIR399* transcription imposed by ID1 is released and miR399 is expected to be produced more in developing leaves. It is then likely that miR399 travels from leaves to roots, where its target gene *ZmPHO2* is downregulated and Pi uptake is enhanced to support the vigorous vegetative growth and extremely delayed flowering of the *id1* mutant. Interestingly, a mutant in the rice ortholog of maize *ID1*, *early heading date2* (*ehd2*), also shows extremely delayed flowering with a giant plant architecture (Matsubara et al. 2008; Wu et al. 2008), which needs nutrients to support this extra vegetative growth. Given the conservation of the *ID1*, miR399, and *PHO2* genes (Bari et al. 2006; Chiou et al. 2006; Matsubara et al. 2008; Wu et al. 2008), this regulatory system might be conserved between maize and rice. However, no *ID1* orthologs have been identified in Arabidopsis (Colasanti et al. 2006). Thus, ID1 might be a monocotyledon-specific factor

that orchestrates plant development and Pi acquisition to maintain growth homeostasis.

The nutrient uptake system may have been altered during maize cultivation to the current soil environments

Maize is well known to require large amounts of nitrogen, phosphorus, and potassium for optimal performance, which puts a high demand on the nutrient uptake system. After diverging from Balsas teosinte 9,000 yr ago through domestication and artificial selection, cultivated maize has been widely adopted as a crop plant in the fertile, highly productive plains of the temperate regions, where it is often grown with the application of fertilizer (Sluyter and Dominguez 2006; Hastorf 2009; Piperno et al. 2009). Compared with modern maize, teosinte grows in the wild in a variable and challenging environment in subtropical southwestern Mexico, where plants are only exposed to occasional and inadequate fertilization from recessional flooding and mineralization (Iltis et al. 1979; Piperno et al. 2007; Hastorf 2009; Zhu et al. 2010). Thus, in addition to the dramatic morphological changes in plant size and architecture, domestication probably also caused alterations in maize metabolism and in its responses to the soil environments, such as nitrogen, potassium, and phosphorus surplus. It is also well known that most breeders involved in maize improvement preferentially focused on yield and disease resistance, which was essential to meet the demand for food due to continued growth of the human population. To increase crop yields, farmers have typically applied large quantities of synthetic fertilizer to the soil, which might induce the degeneration of plant nutrient uptake systems over long periods. In this study, we confirmed that the 5′ UTR of *ZmPHO2*, encoding a central Pi homeostasis regulator, was under selection during maize domestication or cultivation (Fig. 7, A and B; Supplemental Fig. S26). In the context of a partial 5′ UTR (~1.6 kb), the maize allele showed stronger repression by miR399 (Fig. 7D). However, the maize allele of *ZmPHO2* tended to have a higher expression level than the teosinte allele, according to the eQTL data from a maize–teosinte RIL population (Fig. 7E) (Wang et al. 2018) and our investigation with a pair of maize–teosinte NILs across the *ZmPHO2* region (Fig. 7F). Therefore, the expression difference of *ZmPHO2* between maize and teosinte alleles did not result from differences in miR399-mediated RNA cleavage. In our transient coexpression assay (Fig. 7D), only a fragment of the *ZmPHO2* 5′ UTR was used, while additional regulatory elements could have resided in the promoter or elsewhere in the longer 5′ UTR that spans 4 exons intervened by 3 introns (Fig. 2A). Although eQTL mapping with a linkage population identified a *cis*-eQTL for *ZmPHO2*, the limited resolution prevented us from pinpointing the exact location of the causative elements. Thus, it is possible that the detected *cis*-eQTL was located in either the promoter or the 5′ UTR outside of the cloned fragment used for transient coexpression assays. Identifying the causative elements will be necessary to further explain the expression difference of *ZmPHO2* between maize and teosinte alleles. Even so, the higher expression of *ZmPHO2* is consistent with the prevalence of low Pi-sensitive lines in the temperate maize relative to the tropical maize subgroup (Fig. 7, H and I). Thus, the Pi uptake system might have degenerated in modern cultivars, resulting in more low Pi-sensitive maize cultivars, during maize cultivation.

Similar situations might have occurred in maize cultivation in local soils with long-term application of N fertilizer. Indeed, a previous report indicated that the maize progenitor, teosinte, uses nitrogen more efficiently than modern cultivated maize (Gaudin et al. 2011). In rice, high nitrogen supply was shown to have resulted in a prevalence of low nitrogen-use-efficiency (NUE) cultivars (Liu et al. 2021). The allelic variation in *TEOSINTE BRANCHED 1, CYCLOIDEA AND PROLIFERATING CELL FACTOR 19* (*OsTCP19*) contributes to the geographical adaptation to local soil nitrogen. The *OsTCP19-H* allele, which confers higher nitrogen uptake ability, was frequently observed in wild rice populations in natural habitats that usually have low nitrogen content (Liu et al. 2021). However, it has largely been lost in modern cultivars during rice domestication or cultivation in nitrogen-rich regions (Liu et al. 2021), suggesting that *OsTCP19-H* was subjected to relaxed selection pressure due to the nitrogen-rich soil. *DENSE AND ERECT PANICLES 1* (*DEP1*), encoding a G protein that regulates nitrogen signaling and modulation, was previously reported to have been subjected to artificial selection during *O. sativa* spp. *japonica* domestication (Sun et al. 2014). The *DEP1* alleles from *Oryza rufipogon*, the wild ancestor of cultivated rice, confer robust resistance to nitrogen limitation, such that the wild rice shows less sensitivity than *japonica* cultivars (Sun et al. 2014). These data in rice also point to a weakening of the nutrient uptake system in domesticated crop species. New solutions are urgently needed to simultaneously increase yields while maintaining, or preferably decreasing, fertilization use to maximize the efficiency of nutrient use in crops. Otherwise, under conditions of fertilizer shortage, crop yields could be severely impacted in the future. Restoring favorable alleles from the wild ancestor, teosinte, might provide a strategy for improving the nutrient uptake system of cultivated maize and maintaining environmentally sustainable increases in grain yield by avoiding the excessive application of fertilizer.

Materials and methods

Plant materials and growth conditions

The transgenic maize (*Z. mays*) plants of miR399-OE, miR399-STTM, and CRISPR-Cas9 mutant *Zmpho2* were generated by the China National Seed Group Co. Ltd., China, with the inbred line ZZC01 as the receptor line, while the CRISPR-Cas9 mutant *id1-c1* was generated by Functional Genomics and Molecular Breeding of Crops, China Agricultural University, Beijing, with the inbred line LH244 as the receptor line. The heterogeneous inbred family

(MR1451) for developing the near isogenic lines (NILs) around *ZmPHO2* locus was originally generated from a maize–teosinte BC_2S_3 recombinant inbred line (RIL) population derived from a cross between maize inbred line W22 and teosinte accession CIMMYT 8759 (*Z. mays* ssp. *parviglumis*) (Liang et al. 2019). NILs homozygous for W22 and CIMMYT 8759 around the *ZmPHO2* locus were designated *ZmPHO2*-NIL^{maize} and *ZmPHO2*-NIL^{teosinte} and were used for assays. Transgenic miR399-OE and miR399-STTM lines were grown in experimental fields from 2018 to 2021 in the summer in Tieling (Liaoning, 41.8° N, 123.4° E), China, and in the winter in Sanya (Hainan, 18.4° N, 109.2° E), China, for the screening of homozygous plants and bulking up of seeds. Homozygous miR399-OE, miR399-STTM, and the corresponding wild-type plants were grown in the field for phenotypic investigation and in a greenhouse at 25°C, 16-h light/8-h dark photoperiod with light intensity at 130 μmol m^{-2} s^{-1} (metal halide bulb 400 *w*/*d*) for tissue collection. Phenotypic investigation was performed with mature plants in the field, while measurements of *P* content and RNA gel blot assays were performed with seedlings grown in pots (30 cm × 25 cm × 12 cm, length × width × depth) containing vermiculite and organic soil mix (1:1) with full nutrients (N + P_2O_5 + K_2O, 110–1200 mg/kg; PH 5.5–7.5) in the greenhouse.

The *id1-c1* heterozygous mutant, created by CRISPR/Cas9-mediated gene editing, was grown in the experimental field in Tieling (Liaoning, 41.8° N, 123.4° E) or Sanya (Hainan, 18.4° N, 109.2° E) for positive mutant identification and generation of seed stocks, and in a greenhouse for genotyping and tissue collection.

Plasmid construction and genetic transformation

For the construction of the miR399-OE binary vector, 2 stem-loop structures harboring different mature miR399 sequences (i.e. miR399a/c/h and miR399e/i/j) were first inserted into a primary miRNA backbone under the control of the maize *ubiquitin* (*ZmUBI*) promoter in the pOT2-*poly-cis-UN* cloning vector by PCR amplification. After verification by Sanger sequencing and digestion with restriction enzymes, the *UBIpro:miR399:NOS* fragment from the pOT2-*poly-cis-UN-miR399OE* construct was cloned between the *Pac*I and *Mlu*I restriction sites in the destination vector pZZ00026-*PM*, which contains the *Streptomyces hygroscopicus* phosphinothricin acetyltransferase (*BAR*) gene as a selectable marker driven by the cauliflower mosaic virus (CaMV) 35S promoter, via T4 ligase-mediated ligation (Supplemental Fig. S2A).

The miR399-STTM binary vector was prepared following previously described procedures (Tang and Tang 2013; Peng et al. 2018) with some modifications. In brief, the miR399-STTM fragment was first introduced into the pOT2-*poly-cis-UN* cloning vector to be placed under the control of the *ZmUBI* promoter by PCR amplification, *Swa*I digestion, and T4 ligase-mediated ligation. After verification by Sanger sequencing and restriction enzyme digestion, the *UBIpro:miR399-STTM:NOS* fragment from pOT2-*poly-cis-UN-miR399STTM* was cloned between the *Pac*I and *Mlu*I sites in the binary vector pZZ00026-*PM* using T4 ligase (Supplemental Fig. S2B).

To prepare the CRISPR/Cas9 knockout vector for *ID1* or *ZmPHO2*, 2 target sites located in the coding region near the start codon of each gene were selected with the aid of the online tool CRISPR-P (http://crispr.hzau.edu.cn/CRISPR2/) and verified by manual alignment to the maize "B73' reference genome (AGPv5; https://www.maizegdb.org/) (Hufford et al. 2021). After restriction enzyme digestion, the 2 single-guide RNAs (sgRNAs) were integrated into the *Btg*Z1 site to be placed under the control of the maize *U6.1* promoter and the *Bsa*I site to be placed under the control of the maize *U6.2* promoter in the pENTR4-*gRNA1* cloning vector, respectively (Fig. 2; Supplemental Fig. S16). After verification by Sanger sequencing, the *U6pro*-driven gRNA cassette was cloned into the destination vector pZmCas9 by LR recombination.

After verification by Sanger sequencing, the resulting binary construct containing miR399-OE, miR399-STTM, or the sgRNAs with *Cas9* was introduced into Agrobacterium (*Agrobacterium tumefaciens*) strain EHA105 for genetic transformation. To identify mutation events, genomic fragments covering both target sites were amplified from T0 CRISPR/Cas9 plants by PCR. After gel purification, the resulting PCR products were cloned into the pEASY-Blunt cloning vector (TransGen, Beijing, China) and at least ten clones per PCR product were analyzed by Sanger sequencing. Finally, 1 and 3 independent T0 events with large fragment deletions at the target sites were identified for *ID1* and *ZmPHO2*, respectively (Fig. 2; Supplemental Fig. S16).

Quantification of total phosphorus content

Shoots and roots of transgenic miR399-OE and miR399-STTM plants were collected separately as 3 biological replicates at the seedling stage. For each replicate, tissues from more than 5 seedlings were pooled and incubated at 105°C for 30 min. The samples were then dried at 65°C for 3 d, weighed, and milled to a fine powder. Portions (~100 μg) were then digested in 5 mL 65% HNO_3-H_2O_2 at 300°C until the solution became clear. Total phosphorus content was determined by the vanadomolybdophosphoric acid colorimetric method (Westerman 1991). The same protocol was also used to determine total phosphorus content in mature leaves, immature leaves, roots, stems, and leaf sheaths in the *id1-c1* mutant and wild-type plants.

Measurement of relative chlorophyll content

At 15 d after pollination, when the premature senescence syndrome appeared, relative chlorophyll contents were measured from ear leaves with a mobile device, SPAD 502 Plus Chlorophyll Meter (Speactrum Technologies Inc.), which is widely used for the rapid, accurate, and nondestructive measurement of leaf chlorophyll concentrations. Measurements with the SPAD 502 Plus meter produce relative SPAD (soil plant analysis development) values that are proportional to

the amount of chlorophyll present. Three different regions of the leaf (base, middle, and tip) were chosen for measurements. More than 30 plants were used for analysis within an experiment.

Gene expression analysis with RT-qPCR

Total RNA was extracted from mature or immature leaves of the *id1-c1* mutant, miR399-OE transgenic plants, miR399-STTM transgenic plants, and their corresponding wild-type controls using TRIzol reagent (Invitrogen, USA). Genomic DNA removal and first-strand cDNA synthesis were carried out using a TaKaRa first-strand cDNA synthesis kit (TaKaRa, Japan). Quantitative PCR (qPCR) was performed using SYBR Green detection and relative gene expression was determined with the $2^{-\triangle\triangle Ct}$ method (Livak and Schmittgen 2001) from 3 biological replicates. *ZmUBI* was used as the internal control for quantification of transcript levels. Primers used for qPCR are listed in Supplemental Data Set S5.

Small RNA gel blot

Total RNA was isolated by TRIzol reagent from mature and immature leaves of the *id1-c1* mutant and its wild type. Three biological replicates were collected for each genotype with at least 5 leaves pooled per sample. Small RNA was first enriched with a high concentration of NaCl (for each reaction, 50 μL 5 M NaCl and 50 μL 50% PEG8000 were added into 400 μL total RNA), and then, the precipitated RNA was used for RNA gel blot analysis to assess the accumulation of mature miR399 in the *id1-c1* mutant. In brief, a 15% polyacrylamide gel was prepared in 15 mL of gel mixture including 6.3 g urea, 1.5 mL 5×TBE solution and 5.63 mL 40% acrylamide/Bis (29:1) solution, supplied with 100 μL 10% ammonium persulfate (APS), and 10 μL TEMED. A minimum of 10 μg RNA per sample was loaded onto a 15% polyacrylamide gel and resolved at 120 V for 1 h. RNA was transferred from the gel to a nitrocellulose membrane (Bio-Rad) using a semidry transfer apparatus (Bio-Rad). Specific probes labeled with 5′-biotin were hybridized to the membrane. A probe complementary to U6 was used as an internal control. Hybridization was performed at 55°C for 16 h, followed by 3 washes in 20 mL 20×SSC buffer suppled with 0.1% SDS. Signals were detected using a Chemiluminescent Nucleic Acid Detection Module (Thermo Fisher, 89880) with a chemiluminescence imaging system (Clinx Science Instruments Co. Ltd., China). Probe sequences can be found in Supplemental Data Set S5.

Recombinant protein expression and purification, electrophoretic mobility shift assay, and in vitro DNA pull-down assay

To construct the MBP-ID1 vector, the coding sequence (CDS) of *ID1* was first amplified with cDNA prepared from the developing leaves of maize as template, using primers ID1-MBP-F and ID1-MBP-R (Supplemental Data Set S5). The PCR product was then cloned into a version of the pMSCG7 vector with the sequence encoding maltose-binding protein (MBP) at the 5′ end of the cloning site using Gibson assembly; the resulting construct was validated by Sanger sequencing. The empty vector and the version containing the *ID1* CDS were introduced separately into RosettaTM DE3 *E. coli* (Sigma-Aldrich, 70954) for protein expression and purification. Transformed *E. coli* colonies were first cultured to a final OD at 600 nm of 0.7 and then induced with 0.1 mM IPTG (Thermo Fisher Scientific, 15529019) at 16°C for 16 h. The bacterial pellets were collected by centrifugation at 3,972 g with a JLA-16.250 rotor for 10 min at 4°C and resuspended in lysis buffer [100 mM Tris-HCl pH 7.5; 500 mM NaCl; 5 mM 2-mercaptoethanol; 5% (*v*/*v*) glycerol; 20 mM imidazole; 0.1% (*v*/*v*) CA630; 1 mM PMSF; 1×EDTA-free protease inhibitor cocktail]. After sonication (10 s sonication followed with 20 s cooling for 30∼60 times), the recombinant protein was purified with Profinity IMAC Resin, Ni charged (Bio-Rad, 1560133). The protein was eluted with elution buffer [50 mM Tris-HCl, pH 7.5; 500 mM NaCl; 5 mM 2-mercaptoethanol; 5% (*v*/*v*) glycerol; 400 mM imidazole; 0.1% (*v*/*v*) CA630], and the concentration was estimated using a Bradford assay (Quick Start Bradford 1× Dye Reagent #5000205; Bio-Rad).

For EMSA, a 20-μL reaction mixture containing 10× binding buffer (100 mM Tris-HCl, pH 7.5; 500 mM KCl; 10 mM DTT), 20 fmol biotin-labeled probe (Supplemental Data Set S5), recombinant proteins (∼1 μg), and varying amounts of unlabeled probes as competitors was incubated at room temperature for 1 h. DNA–protein complexes were resolved on a 6% polyacrylamide gel and transferred to a charged Hybond-N^+ membrane (GE Healthcare). The membrane was crosslinked by UV light (1,200 mJ), probed with stabilized streptavidin–horseradish peroxidase (HRP), and subsequently detected using a Chemiluminescent Nucleic Acid Detection Module Kit (Thermo Fisher). Membranes were imaged using a ChemiDoc XRS+ camera (BioRad).

For the in vitro DNA pull-down assay, ∼10 pmol of the biotin-labeled probes used in the EMSAs mentioned above was first incubated with 10 μL Dynabeads M-280 streptavidin magnetic beads (Thermo Fisher Scientific) for 15 min at room temperature in 1× B&W buffer (5 mM Tris-HCl pH 7.4, 0.5 mM EDTA, 1 M NaCl). Probe-bound beads were then incubated with the same amount of MBP or MBP-ID1 protein (∼100 ng) in 100 μL binding buffer [10 mM Tris-HCl pH 7.5, 50 mM KCl, 5 mM $MgCl_2$, 2.5% (*v*/*v*) glycerol, 0.05% (*v*/*v*) CA630] containing 10 μg BSA for 1 h at 4°C. The precipitates and 1/5 of the supernatant were boiled in SDS loading buffer and subjected to immunoblot analysis using an anti-MBP monoclonal antibody (New England Biolabs, E8032S, 1:200 dilution), followed by anti-mouse IgG-HRP conjugated antibody (Sigma, A4416, 1:5,000 dilution).

RNA-seq library preparation, sequencing, and data processing

The transgenic lines miR399-OE#2 and miR399-STTM#2, together with the corresponding wild type, were used for

RNA-seq with 3 biological replicates. Mature leaves were collected at the floral transition stage and at least 5 leaves were pooled for each replicate. Total RNA extraction was performed using TRIzol reagent and genomic DNA was removed with recombinant DNase I (Roche) treatment (10 U DNase I per 20 μg total RNA) at 37°C for 1 h. Total RNA quality was verified using an Agilent 2100 Bioanalyzer (Agilent Technologies, Santa Clara, USA) before library preparation. Sequencing libraries were prepared with a NEBNext Ultra II RNA Library Prep Kit for Illumina (NEB) and sequenced on an Illumina HiSeqX10 platform using a 150-bp paired-end sequencing strategy at Novogene Co. Ltd. (Beijing, China). Approximately 25 million high-quality 150-bp paired-end reads were generated from each library.

The raw data were first examined for library quality using the FastQC program (https://github.com/s-andrews/FastQC), which provides a modular set of analyses for a quick impression of the data, including "Per base sequence quality," "Per sequence quality scores," "Per base sequence content," "Per base GC content," "Per sequence GC content," "Per base N content," "Sequence Length Distribution," "Sequence Duplication Levels," "Overrepresented sequences," and "Kmer Content." Raw data after the quality check of FastQC were analyzed using the "pRNASeqTools mrna" pipeline (https://github.com/grubbybio/pRNASeqTools/), which integrates the trimming of low-quality nucleotides, reads alignment, reads/fragments counting, and differential gene expression analysis. In brief, high-quality trimmed reads were mapped to the B73 reference genome (AGPv5; https://www.maizegdb.org/) using STAR 2.7.3a (Dobin et al. 2013) with the parameters "–alignIntronMax 5000 –outSAMmultNmax 1 –outFilterMultimapNmax 50 –outFilterMismatchNoverLmax 0.1". Then, featureCounts (v2.0.0) was employed to count reads mapped to exon regions for each gene with the parameters "-p -B -C -O -s 0" (Liao et al. 2014). Differentially expressed genes (DEGs) were identified with fold change [reads per million (RPM)] ≥ 2 and false discovery rate (FDR) < 0.05 using DESeq2 (Love et al. 2014). Gene Ontology (GO) and Kyoto Encyclopedia of Genes and Genomes (KEGG) enrichment analyses of the DEGs were performed using g:Profiler, a free online platform (https://biit.cs.ut.ee/gprofiler/gost) (Raudvere et al. 2019). GO terms with FDR ≤ 0.05 were retained and deemed significantly enriched.

Small RNA-seq data analysis

The raw small RNA-seq data for the *id1-m1* mutant (accession number PRJNA439244) were downloaded from the National Center for Biotechnology Information Sequence Read Archive (Minow et al. 2018). The 3′ adaptor sequence was detected and removed, and then, size selection (from 18 to 42 nts) was carried out for adaptor-trimmed reads using Cutadapt v1.15 (Martin 2011). The retained reads were mapped to the AGPv5 reference genome for B73 (https://www.maizegdb.org/) using ShortStack v3.8.5 (Johnson et al. 2016). Information on annotated maize miRNAs was obtained from both miRBase v21 (http://www.mirbase.org/) and miRNEST 2.0 (http://rhesus.amu.edu.pl/mirnest/copy/). Adaptor-trimmed reads mapped to specific miRNAs were counted and summarized separately for each size class ranging from 18 to 27 nts. Normalization was performed by calculating the RPM value for each size class, and comparison was carried out using the R package DESeq2 (Love et al. 2014).

Dual-luciferase transient expression assay in maize protoplasts

To examine the regulation of *ZmMIR399* genes by *ID1*, 2-kb promoter fragments for the *ZmMIR399c* and *ZmMIR399j* genes were cloned into the pGreenII 0800-LUC vector, which carries a minimal CaMV promoter (mpCaMV) upstream of the firefly luciferase (*LUC*) coding sequence, to drive *LUC* reporter transcription; the *ID1* coding sequence was cloned into the pGreenII 62-SK vector as effector. Similarly, to validate the relationship between miR399s and *ZmPHO2*, different miR399 precursors were cloned into pGreenII 62-SK as effectors and a ∼1.6-kb 5′ UTR fragment (indicated by the magenta line segment in Fig. 2A) of *ZmPHO2* from B73 was cloned into pGreenII 0800-LUC as the reporter (Supplemental Fig. S7A). To test whether the SNPs around the miR399-binding sites affect miR399-mediated repression of *ZmPHO2*, ∼1.6-kb 5′ UTR fragments (indicated by the magenta line segment in Fig. 2A) of *ZmPHO2* from maize and teosinte were cloned into pGreenII 0800-LUC as reporters, and the miR399c precursor was cloned into pGreenII 62-SK as the effector. The *Renilla* luciferase gene (*REN*) under the control of the 35S promoter in the pGreenII 0800-LUC vector was used as an internal control to correct for differences in protoplast transfection efficiency.

Mesophyll protoplasts were isolated from leaves of 12-d-old etiolated B73 seedlings following a method described previously (Yoo et al. 2007). Each effector/reporter combination was cotransfected into mesophyll protoplasts, using a previously described polyethylene glycol method (Hellens et al. 2005; Yoo et al. 2007). After incubation in the dark for 12 to 16 h, LUC and REN activities were measured using a dual-luciferase reporter assay system (Promega) according to the manufacturer's instructions. Relative LUC activity was calculated by normalizing LUC activity against REN activity. At least 3 technical replicates were performed per construct combination: the same batch of transfected protoplasts was split into different tubes as technical replicates. All experiments were independently performed 3 times. Primers used for plasmid construction are shown in Supplemental Data Set S5.

Agrobacterium-mediated infiltration and fluorescence microscopy in *Nicotiana benthamiana* leaves

To construct *35S:ID1-EYFP*, the *ID1* coding region was PCR-amplified from genomic DNA using primers ID1-TSK-F and ID1-TSK-R (Supplemental Data Set S5). The PCR product was then cloned into TSK108, a pENTRY-D-topo-based

Gateway entry vector. The sequence of the pENTR clone was validated by Sanger sequencing and recombined with the binary vector pGWB641, which contains an *EYFP* sequence at the 3′ end of the recombination site, by Gateway cloning. Similarly, the vector *35S:FIB2-RFP* was prepared in pGWB654 as a nucleolus marker.

For subcellular localization in *N. benthamiana* leaf epidermal cells, Agrobacterium strain GV3101 individually containing the constructs *35S:ID1-EYFP* and *35S:FIB2-RFP* was grown overnight at 28 °C with constant shaking at 200 rpm. The Agrobacterium cells were collected by centrifugation at 3,972 g at room temperature for 10 min. The supernatant was discarded, and the pellet was resuspended in infiltration buffer (10 mM MES pH 5.6, 10 mM $MgCl_2$, 150 mM acetosyringone) to a final OD at 600 nm of 1.0. Subsequently, the Agrobacterium resuspensions of *35S:ID1-EYFP* and *35S:FIB2-RFP* were mixed in equal volume and coinfiltrated into 4-wk-old leaves of *N. benthamiana*. After infiltration, plants were placed under long-day conditions (16-h light/8-h dark, 22 °C) for ∼48 h, and EYFP and RFP fluorescence was observed via confocal microscopy using a Zeiss 710 laser scanning microscope equipped with a Plan-Apochromat 100×/1.4 oil-immersion objective and an Axiocam 506 mono camera (Carl Zeiss, Jena, Germany). To stain the nucleus, the fluorescent stain, 4′ 6-diamidino-2-phenylindole (DAPI), was infiltrated into the leaves, and DAPI fluorescence was observed at 20 min after infiltration via confocal microscopy. The following Zeiss filter sets were used: YFP, exciter 500/25 nm/nm, emitter 535/40 nm/nm; DAPI, exciter 365 nm, emitter 445/50 nm/nm; and RFP, exciter 558 nm, emitter 583/40 nm/nm. Fluorescence images were collected using Zeiss ZEN software.

Chromatin immunoprecipitation (ChIP) assay

The full-length *ID1* coding region was amplified from B73 genomic DNA and subcloned into TSK108. The validated clone was recombined with the binary vector pGWB614, which contains a 3×HA tag at the 3′ end of the recombination site, by Gateway cloning. The fusion construct, *35S:ID1-3×HA*, was introduced into Agrobacterium strain EHA105 for genetic transformation with the maize inbred line ZZC01 as receptor. The leaf tissues of the *35S:ID1-3×HA* transgene-positive line (T1 generation) at the seedling stage were collected to perform chromatin immunoprecipitation (ChIP) assays, with a previously described protocol (Kaufmann et al. 2010) as reference. Sonicated chromatin fragments were immunoprecipitated using anti-HA antibody (Sigma, H6908), and the resulting precipitated chromatin was quantified by qPCR. The percentage input was calculated with the following formula: $2^{-\Delta Ct}$ times 100 and divided by the dilution of the input, in which Δcycle threshold (ΔCt) = (Ct [input] —Ct [ChIP]) (Li et al. 2016). The wild-type (WT) ZZC01 was used as control sample to calculate the fold enrichment.

Nucleotide diversity analysis and test for selection

The third-generation haplotype map data of *Z. mays* (HapMap 3: https://www.panzea.org/) (Bukowski et al. 2018) was downloaded and used to calculate nucleotide diversity along the 10-kb upstream and downstream regions of *ZmMIR399* family genes and *ZmPHO2* in maize, landraces, and teosinte. The population genomic analysis was done with the R package PopGenome (Pfeifer et al. 2014). Sliding windows (window size = 1,000 bp, step size = 100 bp) across the target regions were generated using the function "sliding.window.transform". Nucleotide diversity (π) in each sliding window was calculated for the 3 groups, tropical maize, temperate maize, and teosinte, using the function "diversity.stats." For the analysis of the resequenced ∼1.6-kb region of *ZmPHO2*, multiple sequence alignments were performed using BioEdit v.7.1.3.0 with some manual edits when necessary. Nucleotide diversity was calculated using DnaSP v.5.10.00 with a sliding window size of 100 bp. Coalescent simulations were employed to evaluate whether the loss of nucleotide diversity observed in maize relative to that in teosinte could be explained by a domestication bottleneck alone using Hudson's ms simulator (Hudson 2002). All parameters in the model were set according to previously established values (Wright et al. 2005; Tian et al. 2009; Xu et al. 2017; Liang et al. 2019). The population mutation and population recombination parameters were estimated from the teosinte sequences. A total of 10,000 coalescent simulations were performed.

Acknowledgments

We thank the Instrumental Analysis Center of Shenzhen University for technical assistance.

Author contributions

X.W., X.C., and L.L. designed and supervised the study; X.W., D.Y., YC.L., YM.L., J.H., X.Y., R.H., and Q.X. conducted laboratory experiments, field work, and data analysis; YM.L., H. J., and F.T. created the *id1-c1* mutant by CRISPR/Cas9 technology, generated the near-isogenic lines and provided the DIBOA and DIMBOA standards; X.W. performed the RNA-seq and small RNA-seq data analysis and interpretation; X.W., X.C., and L.L. wrote the manuscript. All authors read and revised the manuscript.

Supplemental data

The following materials are available in the online version of this article.

Supplemental Figure S1. Alignment of mature miR399 sequences in maize and the genomic locations of *ZmMIR399* genes.

Supplemental Figure S2. Schematic diagram of the miR399-OE and miR399-STTM vectors used for genetic transformation.

Supplemental Figure S3. Phenotype of field-grown miR399-overexpressing transgenic plants.

Supplemental Figure S4. Phenotype of leaf necrosis at the seedling stage.

Supplemental Figure S5. Analysis of agronomic traits of 3 independent miR399-overexpressing transgenic lines.

Supplemental Figure S6. Properties of miR399-STTM transgenic plants.

Supplemental Figure S7. Transient coexpression assays in maize protoplasts for validating the relationships between miR399s and *ZmPHO2*.

Supplemental Figure S8. Gene structures of *ZmPHO2* in different versions of maize genome annotations (GRMZM2G381709 in AGPv3; Zm00001d038972 in AGPv4; Zm0001eb295490 in AGPv5).

Supplemental Figure S9. Clustering and principal component analysis (PCA) of experimental samples miR399-OE#3 and miR399-STTM#2 used in RNA-seq.

Supplemental Figure S10. Gene ontology (GO) and KEGG pathway enrichment analyses.

Supplemental Figure S11. The genes involved in the benzoxazinoid biosynthesis pathway and their expression differences between miR399-OEP#3 and miR399-OEN#3.

Supplemental Figure S12. RT-qPCR validation of expression changes of all genes in the benzoxazinoid biosynthesis pathway between the miR399-OE or miR399-STTM transgene-positive lines and the corresponding transgene-negative lines.

Supplemental Figure S13. The relative metabolite content of both DIBOA and DIMBOA between the miR399-OE or miR399-STTM transgene-positive lines and the corresponding transgene-negative lines.

Supplemental Figure S14. Reanalysis of small RNA-seq data downloaded from (Minow et al. 2018).

Supplemental Figure S15. *ZmPHO2* expression in mature leaves (ML) and immature leaves (IL) in the *id1-m1* mutant and wild type (WT).

Supplemental Figure S16. The *id1* knockout line (*id1-c1*) created by CRISPR/Cas9.

Supplemental Figure S17. *ID1* expression levels in transgene-positive (miR399-OEP#3 or miR399-STTMP#2) and the corresponding transgene-negative (miR399-OEN#3 or miR399-STTMN#2) plants.

Supplemental Figure S18. Total phosphorus (P) concentration in the *id1-c1* mutant and wild type (WT) at the floral transition stage.

Supplemental Figure S19. Subcellular localization of the ID1 protein in *Nicotiana benthamiana* leaf epidermal cells.

Supplemental Figure S20. Diagram showing the distribution of ID1-binding motifs in the promoter regions of ten *ZmMIR399* genes.

Supplemental Figure S21. Purification of recombinant ID1 protein.

Supplemental Figure S22. Immunoblot analysis of *35S:ID1-3xHA* transgenic lines.

Supplemental Figure S23. Determination of the levels of miR399 and the long noncoding RNA *PILNCR1*, both of which were known to be upregulated under low-Pi (LP) conditions.

Supplemental Figure S24. Relative *ID1* expression under low-Pi stress conditions.

Supplemental Figure S25. Nucleotide diversity (π) analysis of the genomic regions surrounding *ZmMIR399* family genes in maize, landraces, and teosinte groups with maize HapMap 3 data.

Supplemental Figure S26. Nucleotide diversity (π) analysis of the 5′ regulatory region of *ZmPHO2* in 26 diverse maize inbred lines and 14 teosinte accessions.

Supplemental Figure S27. Expression levels of *ID1*, *ZmPHR1*, *ZmMYB78*, and *PILNCR* genes in mature leaves (ML) and immature leaves (IL) of the *id1-c1* mutant.

Supplemental Table S1. List of 26 diverse maize inbred lines and 14 teosinte accessions used for resequencing the 5′ regulatory region of *ZmPHO2*.

Supplemental Data Set S1. Differentially expressed genes identified between miR399-OE-positive and negative lines.

Supplemental Data Set S2. Differentially expressed genes identified between miR399-STTM-positive and negative lines.

Supplemental Data Set S3. GO and KEGG enrichments for DEGs between miR399-OE-positive and negative lines.

Supplemental Data Set S4. GO and KEGG enrichments for DEGs between miR399-STTM-positive and negative lines.

Supplemental Data Set S5. Primers and probes used in this study.

Supplemental Data Set S6. Results of statistical analysis.

Funding

This research was supported by the National Natural Science Foundation of China (31900446 to X.W.), National Key Research and Development Program of China (2019YFA0903900 to L.L.), the Guangdong Innovation Research Team Foundation (2014ZT05S078 to X.C.), the China Postdoctoral Science Foundation (2018M640823 to X.W.), and a Shenzhen Basic Research General Project (JCYJ20190808112207542 to L.L).

Conflict of interest statement. None declared.

Data availability

The raw RNA-seq data in this study have been submitted to the GenBank database under accession number PRJNA819017.

References

Aguirre-Liguori JA, Gaut BS, Jaramillo-Correa JP, Tenaillon MI, Montes-Hernández S, García-Oliva F, Hearne SJ, Eguiarte LE. Divergence with gene flow is driven by local adaptation to temperature and soil phosphorus concentration in teosinte subspecies (*Zea mays parviglumis* and *Zea mays mexicana*). Mol Ecol. 2019:**28**(11):2814–2830. https://doi.org/10.1111/mec.15098

Andorf C, Beavis WD, Hufford M, Smith S, Suza WP, Wang K, Woodhouse M, Yu J, Lübberstedt T. Technological advances in maize breeding: past, present and future. Theor Appl Genet. 2019:**132**(3):817–849. https://doi.org/10.1007/s00122-019-03306-3

Atkins CA, Smith PMC. Translocation in legumes: assimilates, nutrients, and signaling molecules. Plant Physiol. 2007:**144**(2):550–561. https://doi.org/10.1104/pp.107.098046

Aung K, Lin S-I, Wu C-C, Huang Y-T, Su C-L, Chiou T-J. *Pho2*, a phosphate overaccumulator, is caused by a nonsense mutation in a microRNA399 target gene. Plant Physiol. 2006:**141**(3):1000–1011. https://doi.org/10.1104/pp.106.078063

Baker A, Ceasar SA, Palmer AJ, Paterson JB, Qi W, Muench SP, Baldwin SA. Replace, reuse, recycle: improving the sustainable use of phosphorus by plants. J Exp Bot. 2015:**66**(12):3523–3540. https://doi.org/10.1093/jxb/erv210

Bari R, Datt Pant B, Stitt M, Scheible W-R. *PHO2*, microRNA399, and *PHR1* define a phosphate-signaling pathway in plants. Plant Physiol. 2006:**141**(3):988–999. https://doi.org/10.1104/pp.106.079707

Barnes AC, Rodríguez-Zapata F, Juárez-Núñez KA, Gates DJ, Janzen GM, Kur A, Wang L, Jensen SE, Estévez-Palmas JM, Crow TM, et al. An adaptive teosinte mexicana introgression modulates phosphatidylcholine levels and is associated with maize flowering time. Proc Natl Acad Sci U S A. 2022:**119**(27):e2100036119. https://doi.org/10.1073/pnas.2100036119

Belhaj K, Chaparro-Garcia A, Kamoun S, Patron NJ, Nekrasov V. Editing plant genomes with CRISPR/Cas9. Curr Opin Biotechnol. 2015:**32**:76–84. https://doi.org/10.1016/j.copbio.2014.11.007

Bindraban PS, Dimkpa CO, Pandey R. Exploring phosphorus fertilizers and fertilization strategies for improved human and environmental health. Biol Fertil Soils. 2020:**56**(3):299–317. https://doi.org/10.1007/s00374-019-01430-2

Bologna NG, Voinnet O. The diversity, biogenesis, and activities of endogenous silencing small RNAs in Arabidopsis. Annu Rev Plant Biol. 2014:**65**(1):473–503. https://doi.org/10.1146/annurev-arplant-050213-035728

Breeze E, Harrison E, Mchattie S, Hughes L, Hickman R, Hill C, Kiddle S, Kim Y-S, Penfold CA, Jenkins D, et al. High-resolution temporal profiling of transcripts during Arabidopsis leaf senescence reveals a distinct chronology of processes and regulation. Plant Cell. 2011:**23**(3):873–894. https://doi.org/10.1105/tpc.111.083345

Bukowski R, Guo X, Lu Y, Zou C, He B, Rong Z, Wang B, Xu D, Yang B, Xie C, et al. Construction of the third-generation *Zea mays* haplotype map. Gigascience. 2018:**7**(4):gix134. https://doi.org/10.1093/gigascience/gix134

Bustos R, Castrillo G, Linhares F, Puga MI, Rubio V, Pérez-Pérez J, Solano R, Leyva A, Paz-Ares J. A central regulatory system largely controls transcriptional activation and repression responses to phosphate starvation in Arabidopsis. PLoS Genet. 2010:**6**(9):e1001102. https://doi.org/10.1371/journal.pgen.1001102

Campos-Soriano L, Bundó M, Bach-Pages M, Chiang SF, Chiou TJ, San Segundo B. Phosphate excess increases susceptibility to pathogen infection in rice. Mol Plant Pathol. 2020:**21**(4):555–570. https://doi.org/10.1111/mpp.12916

Chen Z-H, Nimmo GA, Jenkins GI, Nimmo HG. *BHLH32* modulates several biochemical and morphological processes that respond to Pi starvation in Arabidopsis. Biochem J. 2007:**405**(1):191–198. https://doi.org/10.1042/BJ20070102

Chiou T-J, Aung K, Lin S-I, Wu C-C, Chiang S-F, Su C-L. Regulation of phosphate homeostasis by microRNA in Arabidopsis. Plant Cell. 2006:**18**(2):412–421. https://doi.org/10.1105/tpc.105.038943

Colasanti J, Sundaresan V. 'Florigen' enters the molecular age: long-distance signals that cause plants to flower. Trends Biochem Sci. 2000:**25**(5):236–240. https://doi.org/10.1016/S0968-0004(00)01542-5

Colasanti J, Tremblay R, Wong AY, Coneva V, Kozaki A, Mable BK. The maize *INDETERMINATE1* flowering time regulator defines a highly conserved zinc finger protein family in higher plants. BMC Genom. 2006:**7**(1):1–17. https://doi.org/10.1186/1471-2164-7-158

Colasanti J, Yuan Z, Sundaresan V. The indeterminate gene encodes a zinc finger protein and regulates a leaf-generated signal required for the transition to flowering in maize. Cell. 1998:**93**(4):593–603. https://doi.org/10.1016/S0092-8674(00)81188-5

Coneva V, Zhu T, Colasanti J. Expression differences between normal and *indeterminate1* maize suggest downstream targets of ID1, a floral transition regulator in maize. J Exp Bot. 2007:**58**(13):3679–3693. https://doi.org/10.1093/jxb/erm217

Devaiah BN, Karthikeyan AS, Raghothama KG. *WRKY75* transcription factor is a modulator of phosphate acquisition and root development in Arabidopsis. Plant Physiol. 2007a:**143**(4):1789–1801. https://doi.org/10.1104/pp.106.093971

Devaiah BN, Madhuvanthi R, Karthikeyan AS, Raghothama KG. Phosphate starvation responses and gibberellic acid biosynthesis are regulated by the *MYB62* transcription factor in Arabidopsis. Mol Plant. 2009:**2**(1):43–58. https://doi.org/10.1093/mp/ssn081

Devaiah BN, Nagarajan VK, Raghothama KG. Phosphate homeostasis and root development in Arabidopsis are synchronized by the zinc finger transcription factor *ZAT6*. Plant Physiol. 2007b:**145**(1):147–159. https://doi.org/10.1104/pp.107.101691

Devaiah BN, Raghothama KG. Transcriptional regulation of Pi starvation responses by *WRKY75*. Plant Signal Behav. 2007:**2**(5):424–425. https://doi.org/10.4161/psb.2.5.4418

Dobin A, Davis CA, Schlesinger F, Drenkow J, Zaleski C, Jha S, Batut P, Chaisson M, Gingeras TR. STAR: ultrafast universal RNA-seq aligner. Bioinformatics. 2013:**29**(1):15–21. https://doi.org/10.1093/bioinformatics/bts635

Doudna JA, Charpentier E. The new frontier of genome engineering with CRISPR-Cas9. Science. 2014:**346**(6213):1258096. https://doi.org/10.1126/science.1258096

Du Q, Wang K, Zou C, Xu C, Li W-X. The *PILNCR1*-miR399 regulatory module is important for low phosphate tolerance in maize. Plant Physiol. 2018:**177**(4):1743–1753. https://doi.org/10.1104/pp.18.00034

Eyre-Walker A, Gaut RL, Hilton H, Feldman DL, Gaut BS. Investigation of the bottleneck leading to the domestication of maize. Proc Natl Acad Sci U S A. 1998:**95**(8):4441–4446. https://doi.org/10.1073/pnas.95.8.4441

Fang C, Luo J. Metabolic GWAS-based dissection of genetic bases underlying the diversity of plant metabolism. The Plant J. 2019:**97**(1):91–100. https://doi.org/10.1111/tpj.14097

Forde BG. The role of long-distance signalling in plant responses to nitrate and other nutrients. J Exp Bot. 2002:**53**(366):39–43. https://doi.org/10.1093/jexbot/53.366.39

Franco-Zorrilla JM, Valli A, Todesco M, Mateos I, Puga MI, Rubio-Somoza I, Leyva A, Weigel D, García JA, Paz-Ares J. Target mimicry provides a new mechanism for regulation of microRNA activity. Nat Genet. 2007:**39**(8):1033–1037. https://doi.org/10.1038/ng2079

Frey M, Chomet P, Glawischnig E, Stettner C, Grün S, Winklmair A, Eisenreich W, Bacher A, Meeley RB, Briggs SP, et al. Analysis of a chemical plant defense mechanism in grasses. Science. 1997:**277**-(5326):696–699. https://doi.org/10.1126/science.277.5326.696

Frey M, Schullehner K, Dick R, Fiesselmann A, Gierl A. Benzoxazinoid biosynthesis, a model for evolution of secondary metabolic pathways in plants. Phytochemistry. 2009:**70**(15-16):1645–1651. https://doi.org/10.1016/j.phytochem.2009.05.012

Fujii H, Chiou T-J, Lin S-I, Aung K, Zhu J-K. A miRNA involved in phosphate-starvation response in Arabidopsis. Curr Bio. 2005:**15**-(22):2038–2043. https://doi.org/10.1016/j.cub.2005.10.016

Gaudin AC, Mcclymont SA, Raizada MN. The nitrogen adaptation strategy of the wild teosinte ancestor of modern maize. Zea mays subsp. parviglumis. Crop Sci. 2011:**51**(6):2780–2795. https://doi.org/10.2135/cropsci2010.12.0686

Goedert W. Management of the Cerrado soils of Brazil: a review. J Soil Sci. 1983:**34**(3):405–428. https://doi.org/10.1111/j.1365-2389.1983.tb01045.x

González-Muñoz E, Avendaño-Vázquez A-O, Montes R, de Folter S, Andrés-Hernández L, Abreu-Goodger C, Sawers RJ. The maize (*Zea mays* ssp. *mays* var. B73) genome encodes 33 members of the purple acid phosphatase family. Front Plant Sci. 2015:**6**:341. https://doi.org/10.3389/fpls.2015.00341

Hackenberg M, Shi B-J, Gustafson P, Langridge P. Characterization of phosphorus-regulated miR399 and miR827 and their isomirs in

barley under phosphorus-sufficient and phosphorus-deficient conditions. BMC Plant Bio. 2013:**13**(214): 1–17. https://doi.org/10.1186/1471-2229-13-214

Hastorf CA. Rio Balsas most likely region for maize domestication. Proc Natl Acad Sci U S A. 2009:**106**(13):4957–4958. https://doi.org/10.1073/pnas.0900935106

Hellens RP, Allan AC, Friel EN, Bolitho K, Grafton K, Templeton MD, Karunairetnam S, Gleave AP, Laing WA. Transient expression vectors for functional genomics, quantification of promoter activity and RNA silencing in plants. Plant Methods. 2005:**1**(1):13. https://doi.org/10.1186/1746-4811-1-13

Hu B, Zhu C, Li F, Tang J, Wang Y, Lin A, Liu L, Che R, Chu C. *LEAF TIP NECROSIS1* plays a pivotal role in the regulation of multiple phosphate starvation responses in rice. Plant Physiol. 2011:**156**(3): 1101–1115. https://doi.org/10.1104/pp.110.170209

Hudson RR. Generating samples under a Wright-Fisher neutral model of genetic variation. Bioinformatics. 2002:**18**(2):337–338. https://doi.org/10.1093/bioinformatics/18.2.337

Huen A, Bally J, Smith P. Identification and characterisation of microRNAs and their target genes in phosphate-starved *Nicotiana benthamiana* by small RNA deep sequencing and 5′RACE analysis. BMC Genom. 2018:**19**(1):940. https://doi.org/10.1186/s12864-018-5258-9

Hufford MB, Seetharam AS, Woodhouse MR, Ou S, Liu J, Ricci WA, Guo T, Olson A, Qiu Y, Della Coletta R, et al. De novo assembly, annotation, and comparative analysis of 26 diverse maize genomes. Science. 2021:**373**(6555):655–662. https://doi.org/10.1126/science.abg5289

Iltis HH, Doebley JF, Guzmán R, Pazy B. *Zea diploperennis* (Gramineae): a new teosinte from Mexico. Science. 1979:**203**(4376): 186–188. https://doi.org/10.1126/science.203.4376.186

Johnson NR, Yeoh JM, Coruh C, Axtell MJ. Improved placement of multi-mapping small RNAs. G3. 2016:**6**(7):2103–2111. https://doi.org/10.1534/g3.116.030452

Kasai A, Kanehira A, Harada T. Mir172 can move long distance in *Nicotiana benthamiana*. Open Plant Sci J. 2010:**4**(1):1–6. https://doi.org/10.2174/1874294701004010001

Kaufmann K, Muino JM, Sterås M, Farinelli L, Krajewski P, Angenent GC. Chromatin immunoprecipitation (ChIP) of plant transcription factors followed by sequencing (ChIP-SEQ) or hybridization to whole genome arrays (ChIP-CHIP). Nat Protoc. 2010:**5**(3):457–472. https://doi.org/10.1038/nprot.2009.244

Khan MJ, Muhammad D, Fahad S, Adnan M, Wahid F, Alamri S, Khan F, Dawar KM, Irshad I, Danish S, et al. Phosphorus nutrient management through synchronization of application methods and rates in wheat and maize crops. Plants. 2020:**9**(10):1389. https://doi.org/10.3390/plants9101389

Kozaki A, Hake S, Colasanti J. The maize *ID1* flowering time regulator is a zinc finger protein with novel DNA binding properties. Nucleic Acids Res. 2004:**32**(5):1710–1720. https://doi.org/10.1093/nar/gkh337

Kremling KA, Chen S-Y, Su M-H, Lepak NK, Romay MC, Swarts KL, Lu F, Lorant A, Bradbury PJ, Buckler ES. Dysregulation of expression correlates with rare-allele burden and fitness loss in maize. Nature. 2018:**555**(7697):520–523. https://doi.org/10.1038/nature25966

Li Z, Gao Q, Liu Y, He C, Zhang X, Zhang J. Overexpression of transcription factor *ZmPTF1* improves low phosphate tolerance of maize by regulating carbon metabolism and root growth. Planta. 2011:**233**(6):1129–1143. https://doi.org/10.1007/s00425-011-1368-1

Li S, Liu L, Li S, Gao L, Zhao Y, Kim YJ, Chen X. SUVH1, A Su (var) 3-9 family member, promotes the expression of genes targeted by DNA methylation. Nucleic Acids Res. 2016:**44**(2):608–620. https://doi.org/10.1093/nar/gkv958

Li S, Wang X, Xu W, Liu T, Cai C, Chen L, Clark CB, Ma J. Unidirectional movement of small RNAs from shoots to roots in interspecific heterografts. Nat Plants. 2021:**7**(1):50–59. https://doi.org/10.1038/s41477-020-00829-2

Li S, Ying Y, Secco D, Wang C, Narsai R, Whelan J, Shou H. Molecular interaction between *PHO2* and *GIGANTEA* reveals a new crosstalk between flowering time and phosphate homeostasis in *Oryza sativa*. Plant Cell Environ. 2017:**40**(8):1487–1499. https://doi.org/10.1111/pce.12945

Liang Y, Liu Q, Wang X, Huang C, Xu G, Hey S, Lin H-Y, Li C, Xu D, Wu L, et al. *ZmMADS69* functions as a flowering activator through the *ZmRap2.7-ZCN 8* regulatory module and contributes to maize flowering time adaptation. New Phytol. 2019:**221**(4):2335–2347. https://doi.org/10.1111/nph.15512

Liao Y, Smyth GK, Shi W. Featurecounts: an efficient general purpose program for assigning sequence reads to genomic features. Bioinformatics. 2014:**30**(7):923–930. https://doi.org/10.1093/bioinformatics/btt656

Lin S-I, Chiang S-F, Lin W-Y, Chen J-W, Tseng C-Y, Wu P-C, Chiou T-J. Regulatory network of microRNA399 and *PHO2* by systemic signaling. Plant Physiol. 2008:**147**(2):732–746. https://doi.org/10.1104/pp.108.116269

Liu T-Y, Huang T-K, Tseng C-Y, Lai Y-S, Lin S-I, Lin W-Y, Chen J-W, Chiou T-J. *PHO2*-dependent degradation of *PHO1* modulates phosphate homeostasis in Arabidopsis. Plant Cell. 2012:**24**(5): 2168–2183. https://doi.org/10.1105/tpc.112.096636

Liu Y, Wang H, Jiang Z, Wang W, Xu R, Wang Q, Zhang Z, Li A, Liang Y, Ou S, et al. Genomic basis of geographical adaptation to soil nitrogen in rice. Nature. 2021:**590**(7847):600–605. https://doi.org/10.1038/s41586-020-03091-w

Livak KJ, Schmittgen TD. Analysis of relative gene expression data using real-time quantitative PCR and the $2^{-\Delta\Delta CT}$ method. Methods. 2001:**25**(4):402–408. https://doi.org/10.1006/meth.2001.1262

López-Arredondo DL, Leyva-González MA, González-Morales SI, López-Bucio J, Herrera-Estrella L. Phosphate nutrition: improving low-phosphate tolerance in crops. Annu Rev Plant Biol. 2014:**65**(1): 95–123. https://doi.org/10.1146/annurev-arplant-050213-035949

Love MI, Huber W, Anders S. Moderated estimation of fold change and dispersion for RNA-seq data with DESeq2. Genome Biol. 2014:**15**(12):1–21. https://doi.org/10.1186/s13059-014-0550-8

Luo B, Ma P, Nie Z, Zhang X, He X, Ding X, Feng X, Lu Q, Ren Z, Lin H, et al. Metabolite profiling and genome-wide association studies reveal response mechanisms of phosphorus deficiency in maize seedling. Plant J. 2019:**97**(5):947–969. https://doi.org/10.1111/tpj.14160

Lynch JP, Brown KM. Topsoil foraging-an architectural adaptation of plants to low phosphorus availability. Plant Soil. 2001:**237**(2): 225–237. https://doi.org/10.1023/A:1013324727040

Ma B, Zhang L, Gao Q, Wang J, Li X, Wang H, Liu Y, Lin H, Liu J, Wang X, et al. A plasma membrane transporter coordinates phosphate reallocation and grain filling in cereals. Nat Genet. 2021:**53**(6):906–915. https://doi.org/10.1038/s41588-021-00855-6

Ma X, Zhang Q, Zhu Q, Liu W, Chen Y, Qiu R, Wang B, Yang Z, Li H, Lin Y, et al. A robust CRISPR/Cas9 system for convenient, high-efficiency multiplex genome editing in monocot and dicot plants. Mol Plant. 2015:**8**(8):1274–1284. https://doi.org/10.1016/j.molp.2015.04.007

Maeda Y, Konishi M, Kiba T, Sakuraba Y, Sawaki N, Kurai T, Ueda Y, Sakakibara H, Yanagisawa S. A NIGT1-centred transcriptional cascade regulates nitrate signalling and incorporates phosphorus starvation signals in Arabidopsis. Nat Commun. 2018:**9**(1):1–14. https://doi.org/10.1038/s41467-018-03832-6

Marschner H. Mineral nutrition of higher plants. San Diago: Academic Press. Inc.; 1995.

Martin M. Cutadapt removes adapter sequences from high-throughput sequencing reads. EMBnet J. 2011:**17**(1):10–12. https://doi.org/10.14806/ej.17.1.200

Martín-Robles N, Morente-López J, Freschet GT, Poorter H, Roumet C, Milla R. Root traits of herbaceous crops: pre-adaptation to cultivation or evolution under domestication? Funct Ecol. 2019:**33**(2): 273–285. https://doi.org/10.1111/1365-2435.13231

Matsubara K, Yamanouchi U, Wang ZX, Minobe Y, Izawa T, Yano M. *Ehd2*, a rice ortholog of the maize *INDETERMINATE1* gene, promotes

flowering by up-regulating *Ehd1*. Plant Physiol. 2008:**148**(3): 1425–1435. https://doi.org/10.1104/pp.108.125542

Matsuoka Y, Vigouroux Y, Goodman MM, Sanchez J, Buckler E, Doebley J. A single domestication for maize shown by multilocus microsatellite genotyping. Proc Natl Acad Sci U S A. 2002:**99**(9): 6080–6084. https://doi.org/10.1073/pnas.052125199

Minow M, vila LM, Turner K, Ponzoni E, Mascheretti I, Dussault FM, Lukens L, Rossi V, Colasanti J. Distinct gene networks modulate floral induction of autonomous maize and photoperiod-dependent teosinte. J Exp Bot. 2018:**69**(12):2937–2952. https://doi.org/10.1093/jxb/ery110

Pant BD, Buhtz A, Kehr J, Scheible WR. MicroRNA399 is a long-distance signal for the regulation of plant phosphate homeostasis. The Plant J. 2008:**53**(5):731–738. https://doi.org/10.1111/j.1365-313X.2007.03363.x

Peng T, Qiao M, Liu H, Teotia S, Zhang Z, Zhao Y, Wang B, Zhao D, Shi L, Zhang C, et al. A resource for inactivation of microRNAs using short tandem target mimic technology in model and crop plants. Mol Plant. 2018:**11**(11):1400–1417. https://doi.org/10.1016/j.molp.2018.09.003

Pfeifer B, Wittelsbürger U, Ramos-Onsins SE, Lercher MJ. Popgenome: an efficient Swiss army knife for population genomic analyses in R. Mol Biol Evo. 2014:**31**(7):1929–1936. https://doi.org/10.1093/molbev/msu136

Piperno DR, Moreno JE, Iriarte J, Holst I, Lachniet M, Jones JG, Ranere AJ, Castanzo R. Late Pleistocene and Holocene environmental history of the Iguala Valley, central Balsas watershed of Mexico. Proc Natl Acad Sci U S A. 2007:**104**(29):11874–11881. https://doi.org/10.1073/pnas.0703442104

Piperno DR, Ranere AJ, Holst I, Iriarte J, Dickau R. Starch grain and phytolith evidence for early ninth millennium BP maize from the Central Balsas River Valley, Mexico. Proc Natl Acad Sci U S A. 2009:**106**(13):5019–5024. https://doi.org/10.1073/pnas.0812525106

Qaswar M, Dongchu L, Jing H, Tianfu H, Ahmed W, Abbas M, Lu Z, Jiangxue D, Khan ZH, Ullah S, et al. Interaction of liming and long-term fertilization increased crop yield and phosphorus use efficiency (PUE) through mediating exchangeable cations in acidic soil under wheat–maize cropping system. Sci Rep. 2020:**10**(1):1–12. https://doi.org/10.1038/s41598-020-76892-8

Raghothama K. Phosphate acquisition. Annu Rev Plant Bio. 1999:**50**(1): 665–693. https://doi.org/10.1146/annurev.arplant.50.1.665

Raudvere U, Kolberg L, Kuzmin I, Arak T, Adler P, Peterson H, Vilo J. G: Profiler: a web server for functional enrichment analysis and conversions of gene lists (2019 update). Nucleic Acids Res. 2019:**47**(W1): W191–W1W8. https://doi.org/10.1093/nar/gkz369

Reeves G, Tripathi A, Singh P, Jones MR, Nanda AK, Musseau C, Craze M, Bowden S, Walker JF, Bentley AR, et al. Monocotyledonous plants graft at the embryonic root-shoot interface. Nature. 2022:**602**(7896):280–286. https://doi.org/10.1038/s41586-021-04247-y

Rubio V, Linhares F, Solano R, Martín AC, Iglesias J, Leyva A, Paz-Ares J. A conserved MYB transcription factor involved in phosphate starvation signaling both in vascular plants and in unicellular algae. Genes Dev. 2001:**15**(16):2122–2133. https://doi.org/10.1101/gad.204401

Schachtman DP, Shin R. Nutrient sensing and signaling: NPKS. Annu Rev Plant Biol. 2007:**58**(1):47–69. https://doi.org/10.1146/annurev.arplant.58.032806.103750

Sega P, Kruszka K, Szewc Ł, Szweykowska-Kulińska Z, Pacak A. Identification of transcription factors that bind to the 5′-UTR of the barley *PHO2* gene. Plant Mol Biol. 2020:**102**(1-2):73–88. https://doi.org/10.1007/s11103-019-00932-9

Singleton WR. Inheritance of indeterminate growth in maize. J Hered. 1946:**37**(2):61–64. https://doi.org/10.1093/oxfordjournals.jhered.a105582

Sluyter A, Dominguez G. Early maize (*Zea mays L.*) cultivation in Mexico: dating sedimentary pollen records and its implications. Proc Natl Acad Sci U S A. 2006:**103**(4):1147–1151. https://doi.org/10.1073/pnas.0510473103

Stefanovic A, Ribot C, Rouached H, Wang Y, Chong J, Belbahri L, Delessert S, Poirier Y. Members of the *PHO1* gene family show limited functional redundancy in phosphate transfer to the shoot, and are regulated by phosphate deficiency via distinct pathways. The Plant J. 2007:**50**(6):982–994. https://doi.org/10.1111/j.1365-313X.2007.03108.x

Stigter KA, Plaxton WC. Molecular mechanisms of phosphorus metabolism and transport during leaf senescence. Plants. 2015:**4**(4): 773–798. https://doi.org/10.3390/plants4040773

Sun H, Qian Q, Wu K, Luo J, Wang S, Zhang C, Ma Y, Liu Q, Huang X, Yuan Q, et al. Heterotrimeric G proteins regulate nitrogen-use efficiency in rice. Nat Genet. 2014:**46**(6):652–656. https://doi.org/10.1038/ng.2958

Tang G, Tang X. Short tandem target mimic: a long journey to the engineered molecular landmine for selective destruction/blockage of microRNAs in plants and animals. J Genet Genom. 2013:**40**(6): 291–296. https://doi.org/10.1016/j.jgg.2013.02.004

Tang G, Yan J, Gu Y, Qiao M, Fan R, Mao Y, Tang X. Construction of short tandem target mimic (STTM) to block the functions of plant and animal microRNAs. Methods. 2012:**58**(2):118–125. https://doi.org/10.1016/j.ymeth.2012.10.006

Tian F, Stevens NM, Buckler ES. Tracking footprints of maize domestication and evidence for a massive selective sweep on chromosome 10. Proc Natl Acad Sci U S A. 2009:**106**(supplement_1):9979–9986. https://doi.org/10.1073/pnas.0901122106

Vance CP, Uhde-Stone C, Allan DL. Phosphorus acquisition and use: critical adaptations by plants for securing a nonrenewable resource. New Phytol. 2003:**157**(3):423–447. https://doi.org/10.1046/j.1469-8137.2003.00695.x

Vasconcelos M, Figueiredo J, Oliveira M, Parentoni S, Marriel I, Raghothama K. Expression analysis of phosphate induced genes in contrasting maize genotypes for phosphorus use efficiency. Braz J Biol. 2022:**82**:e261797. https://doi.org/10.1590/1519-6984.261797

Wang X, Bai J, Liu H, Sun Y, Shi X, Ren Z. Overexpression of a maize transcription factor *ZmPHR1* improves shoot inorganic phosphate content and growth of Arabidopsis under low-phosphate conditions. Plant Mol Biol Rep. 2013b:**31**(3):665–677. https://doi.org/10.1007/s11105-012-0534-3

Wang X, Chen Q, Wu Y, Lemmon ZH, Xu G, Huang C, Liang Y, Xu D, Li D, Doebley JF, et al. Genome-wide analysis of transcriptional variability in a large maize-teosinte population. Mol Plant. 2018:**11**(3): 443–459. https://doi.org/10.1016/j.molp.2017.12.011

Wang J, Pan W, Nikiforov A, King W, Hong W, Li W, Han Y, Patton-Vogt J, Shen J, Cheng L. Identification of two glycerophosphodiester phosphodiesterase genes in maize leaf phosphorus remobilization. The Crop J. 2021:**9**(1):95–108. https://doi.org/10.1016/j.cj.2020.05.004

Wang J, Sun J, Miao J, Guo J, Shi Z, He M, Chen Y, Zhao X, Li B, Han F, et al. A phosphate starvation response regulator *Ta-PHR1* is involved in phosphate signalling and increases grain yield in wheat. Ann Bot. 2013a:**111**(6):1139–1153. https://doi.org/10.1093/aob/mct080

Westerman RL. Soil testing and plant analysis. 3rd ed. Madison: Soil Science Society of America; 1991.

Wright SI, Bi IV, Schroeder SG, Yamasaki M, Doebley JF, McMullen MD, Gaut BS. The effects of artificial selection on the maize genome. Science. 2005:**308**(5726):1310–1314. https://doi.org/10.1126/science.1107891

Wu C, You C, Li C, Long T, Chen G, Byrne ME, Zhang Q. *RID1*, Encoding a Cys2/His2-type zinc finger transcription factor, acts as a master switch from vegetative to floral development in rice. Proc Natl Acad Sci U S A. 2008:**105**(35):12915–12920. https://doi.org/10.1073/pnas.0806019105

Xu F, Liu Q, Chen L, Kuang J, Walk T, Wang J, Liao H. Genome-wide identification of soybean microRNAs and their targets reveals their

organ-specificity and responses to phosphate starvation. BMC Genom. 2013:**14**(1):1–30. https://doi.org/10.1186/1471-2164-14-66

Xu G, Wang X, Huang C, Xu D, Li D, Tian J, Chen Q, Wang C, Liang Y, Wu Y, et al. Complex genetic architecture underlies maize tassel domestication. New Phytol. 2017:**214**(2):852–864. https://doi.org/10.1111/nph.14400

Yan J, Gu Y, Jia X, Kang W, Pan S, Tang X, Chen X, Tang G. Effective small RNA destruction by the expression of a short tandem target mimic in Arabidopsis. Plant Cell. 2012:**24**(2):415–427. https://doi.org/10.1105/tpc.111.094144

Yi K, Wu Z, Zhou J, Du L, Guo L, Wu Y, Wu P. *OsPTF1*, a novel transcription factor involved in tolerance to phosphate starvation in rice. Plant Physiol. 2005:**138**(4):2087–2096. https://doi.org/10.1104/pp.105.063115

Yoo S-D, Cho Y-H, Sheen J. Arabidopsis mesophyll protoplasts: a versatile cell system for transient gene expression analysis. Nat Protoc. 2007:**2**(7):1565–1572. https://doi.org/10.1038/nprot.2007.199

Zhang L, Chia J-M, Kumari S, Stein JC, Liu Z, Narechania A, Maher CA, Guill K, McMullen MD, Ware D. A genome-wide characterization of microRNA genes in maize. PLoS Genet. 2009:**5**(11):e1000716. https://doi.org/10.1371/journal.pgen.1000716

Zhou J, Jiao F, Wu Z, Li Y, Wang X, He X, Zhong W, Wu P. *OsPHR2* is involved in phosphate-starvation signaling and excessive phosphate accumulation in shoots of plants. Plant Physiol. 2008:**146**(4):1673–1686. https://doi.org/10.1104/pp.107.111443

Zhu J, Zhang C, Lynch JP. The utility of phenotypic plasticity of root hair length for phosphorus acquisition. Funct Plant Biol. 2010:**37**(4):313–322. https://doi.org/10.1071/FP09197